Aus der Klinik und Poliklinik für Nuklearmedizin
der Ludwig-Maximilians-Universität München

Direktor: Prof. Dr. med. P. Bartenstein

Multimodale Bildgebung in der pädiatrischen Onkologie

Dissertation

zum Erwerb des Doktorgrades der Humanmedizin
an der medizinischen Fakultät
der Ludwig-Maximilians-Universität München

vorgelegt von
Henriette Ingrid Melzer

aus
Witzenhausen

Jahr
2013

Mit Genehmigung der medizinischen Fakultät der
Ludwig-Maximilians-Universität München

Berichterstatter:	**Priv.-Doz. Dr. med. T. Pfluger**
Mitberichterstatter:	**Prof. Dr. Joachim-Ulrich Walther** **Priv.-Doz. Dr. Sabine Weckbach**
Dekan:	**Prof. Dr. med. Dr. h.c. M. Reiser, FACR, FRCR**
Tag der mündlichen Prüfung:	**14.03.2013**

Die vorliegende kumulative Dissertation umfasst zwei Manuskripte, die mit Genehmigung des Promotionsausschusses der medizinischen Fakultät der Ludwig-Maximilians-Universität München vorab publiziert wurden.

Diagnostic value of combined ^{18}F-FDG PET/MRI for staging and restaging in paediatric oncology.

Pfluger T, **Melzer HI**, Mueller WP, Coppenrath E, Bartenstein P, Albert MH, Schmid I. Eur J Nucl Med Mol Imaging. 2012 Nov;39(11):1745-55.

^{123}I-MIBG scintigraphy/SPECT versus ^{18}F-FDG PET in paediatric neuroblastoma.

Melzer HI, Coppenrath E, Schmid I, Albert MH, von Schweinitz D, Tudball C, Bartenstein P, Pfluger T. Eur J Nucl Med Mol Imaging. 2011 Sep;38(9):1648-58.

Inhaltsverzeichnis

1. Einleitung

1.1 Relevanz für die pädiatrische Onkologie

Maligne Erkrankungen stellen im Kindesalter nach Unfällen die zweithäufigste Todesursache dar. Insgesamt sind jedoch Kinder sehr viel seltener betroffen als Erwachsene – nur 2 % aller Tumorerkrankungen fallen ins Kindesalter [1]. Im Zeitraum von 1975 bis 2006 konnte die Mortalitätsrate aller onkologischen Erkrankungen im Kindesalter um mehr als 50 % gesenkt werden [2]. Neben neuen Therapieansätzen ist besonders die verbesserte Diagnostik für diesen Erfolg maßgebend. Tritt eine maligne Erkrankung auf, ist für die Primärdiagnostik ein schnelles und möglichst exaktes Staging notwendig, um die genaue anatomische Tumorausbreitung und die Metastasen zu erfassen. Anschließend wird ein adäquates, stadienabhängiges Therapiekonzept erstellt. Im Verlauf der Tumortherapie (Follow-up) sind aussagekräftige Untersuchungen zum Therapiemonitoring und zur frühzeitigen Rezidiverkennung von entscheidender therapeutischer Relevanz [3].

1.2 Onkologische Bildgebung

In der onkologischen Pädiatrie wird – wie in den bildgebenden Fächern üblich – grundsätzlich zwischen der morphologischen und funktionellen Darstellung unterschieden. Der Vorteil der morphologischen Verfahren wie der Computertomographie (CT), der Magnetresonanztomographie (MRT) und des Ultraschalls (US) liegt dabei in der exakten Darstellung anatomischer Strukturen. Voraussetzung für die fehlerfreie Interpretation ist die genaue Kenntnis der physiologischen anatomischen Verhältnisse. Aussagen über bestimmte Stoffwechselwege sowie über die Stoffwechselaktivität in relevanten Geweben und Organen können mit morphologischen Verfahren im Allgemeinen nicht getroffen werden. Dies gelingt mit Hilfe funktioneller Verfahren wie der Positronenemissionstomographie (PET), der planaren Szintigraphie und der Single Photon Emission Computer Tomography (SPECT). Je nach verwendetem Radiotracer können Stoffwechselauffälligkeiten generalisiert oder in speziellen Geweben sichtbar gemacht werden. Der entscheidende Nachteil funktioneller Untersuchungsmodalitäten besteht in ihrer geringen räumlichen Auflösung, die eine Zuordnung von fokalen metabolischen Auffälligkeiten zu bestimmten anatomischen Strukturen erheblich beeinträchtigt [4], [5], [6]. In den folgenden Abschnitten wird kurz auf die grundlegenden Prinzipien der Bildgebungsmodalitäten dieser Arbeit eingegangen.

1.3 ^{18}F-Fluordesoxyglukose Positronenemissionstomographie

Das zentrale Verbindungsglied der beiden zugrunde liegenden Veröffentlichungen dieser Dissertation ist die ^{18}F-Fluordesoxyglukose Positronenemissionstomographie (^{18}F-FDG-PET)-Diagnostik bei kindlichen Tumoren. Für diese Bildgebungsmodalität wird ein Radiopharmakon, bestehend aus der radioaktiv markierten Substanz und einem Trägermolekül, intravenös appliziert. In der Onkologie wird hierfür häufig radioaktiv markierte Fluordesoxyglukose verwendet, die in den Glukosestoffwechsel der Zellen eingeschleust und nur sehr langsam verstoffwechselt wird (metabolic trapping). Diese reichert sich bevorzugt in Gewebe mit erhöhter Stoffwechselrate wie beispielsweise in maligne entartetem Gewebe an [7]. Das Radiopharmakon emittiert Positronen, die an Elektronen im umliegenden Gewebe abgebremst werden und mit diesen wechselwirken (Annihilation). Dabei werden zwei Photonen mit einer Energie von 511 keV in einem Winkel von 180 ° ausgesandt (Vernichtungsstrahlung). Ein um den Patienten gelagerter Detektorring registriert die eintreffenden Gammaquanten. Durch Koinzidenzschaltung wird nur bei gleichzeitigem Eintreffen zweier Photonen ein Bildsignal erzeugt und entsprechend der geometrischen Verhältnisse die anatomisch-topographische Zuordnung des Positronenzerfalls berechnet [5].

1.4 Magnetresonanztomographie

Die Magnetresonanztomographie (MRT) ist ein Schnittbildverfahren ohne Verwendung ionisierender Strahlung [8]. Das Verfahren beruht größtenteils auf dem Kernspin von Protonen im menschlichen Körper, die sich unter Einwirkung eines äußeren Magnetfeldes parallel ausrichten und mit einer bestimmten Frequenz schwingen. Bei Wegfall des äußeren Magnetfeldes geben die Protonen die aufgenommene Energie wieder ab, die registriert und mittels Umrechnung zur Bildgebung genutzt werden kann [5].

1.5 ^{123}I-Metaiodbenzylguanidin-Szintigraphie/SPECT

Die ^{123}I-Metaiodbenzylguanidin (^{123}I-MIBG)-Szintigraphie dient der Diagnostik katecholaminproduzierender Tumoren des peripheren sympathischen Nervensystems [9]. Dabei wird das applizierte Noradrenalinanalogon ^{123}I-MIBG über einen präsynaptischen Transporter in die Tumorzellen aufgenommen und in Vesikeln gespeichert [9]. Das an MIBG gekoppelte ^{123}I-Iod ist ein Gamma-Strahler. Die aus dem Körper austretende Strahlung wird mit einer Gammakamera detektiert und mittels eines Szintillationskristalls in Lichtblitze umgewandelt. Ein Photomultiplier führt zu einer Verstärkung des Signals um den Faktor 10^5, wodurch ein elektrisches Signal entsteht. Die Single Photon Emission Computer Tomography (SPECT)

dient dazu, aus den Messdaten sagittale, axiale und coronare Aufnahmen zu rekonstruieren. Dafür rotieren eine oder mehrere Gammakameras um den Patienten. Die räumliche Auflösung ist gering, jedoch werden Überlagerungseffekte wie bei der planaren Szintigraphie vermieden [5].

1.6 Statistik

Die statistische Beurteilung der verschiedenen bildgebenden Verfahren erfolgte in beiden Studien anhand der Sensitivität und Spezifität. Die Sensitivität ist ein Parameter für die Empfindlichkeit eines Untersuchungsverfahrens und errechnet sich aus dem Quotienten der korrekt positiven Resultate und der Summe der richtig positiven und falsch negativen Befunde. Die Sensitivität kann damit als Maß für die Wahrscheinlichkeit des richtigen Erkennens einer malignen Erkrankung beziehungsweise einer malignen Läsion betrachtet werden. Eine Untersuchungsmethode mit hoher Sensitivität erfasst nahezu alle tatsächlichen Tumorläsionen, jedoch ist die Rate der falsch positiven Befunde unter Umständen hoch. In der Onkologie sind die Existenz und das Erkennen von Metastasen von entscheidender Bedeutung für die Klassifikation der malignen Erkrankung und für die Wahl des am besten geeigneten Therapiekonzepts. Daher spielt die Sensitivität der verwendeten Bildgebungsverfahren in beiden zugrunde liegenden Studien in der Primärdiagnostik eine zentrale Rolle.
Im Follow-up einer onkologischen Erkrankung besteht die Anforderung an die bildgebenden Verfahren dagegen vor allem in der zuverlässigen Erkennung von Rezidiven, die sicher von residuellen Läsionen nach operativer Versorgung oder Chemotherapie abgegrenzt werden müssen. Die genaue Anzahl der Läsionen und Metastasen ist im Follow-up dagegen weniger entscheidend. Dies gelingt am besten mit Bildgebungsmodalitäten, die über eine hohe Spezifität, das heißt über eine hohe Wahrscheinlichkeit für das Erkennen negativer Befunde, verfügen. Die Spezifität ist dabei der Quotient der korrekt negativen Resultate und der Summe aus richtig negativen und falsch positiven Befunden. Für den Vergleich von Sensitivität und Spezifität der einzelnen Bildgebungsmethoden wurde der positive Likelihood-Quotient bestimmt und mit Hilfe des McNemars Chi-square Tests erfolgte die statistische Analyse. Verwendet wurde das „Statistical Package for 230 the Social Sciences (SPSS, version 15.0, Chicago, IL, 231 USA)". Das Signifikanzniveau betrug $p<0.05$.

1.7 Fragestellung

Die ^{18}F-FDG-PET ist heutzutage eine etablierte Untersuchungsmodalität in der pädiatrischen Onkologie – in der Erwachsenenonkologie wird die ^{18}F-FDG-PET bereits routinemäßig in Kombination mit weiteren Bildgebungsmodalitäten eingesetzt [10], [11]. Weltweit liegen allerdings nur wenige Studien aus der Kinderonkologie zu Kombinationsmöglichkeiten der ^{18}F-FDG-PET mit anderen Bildgebungsmodalitäten vor. Beide dieser Arbeit zugrunde liegenden Studien kombinieren die ^{18}F-FDG-PET mit einem weiteren Bildgebungsverfahren – erstens einer morphologischen Modalität (MRT) und zweitens einer weiteren funktionellen Bildgebungsmodalität (^{123}I-MIBG-Szintigraphie) – und evaluieren die diagnostische Zusatzinformation.

1.8 Kombinierte ^{18}F-FDG-PET/MRT verglichen mit ^{18}F-FDG-PET und MRT

Diagnostic value of combined ^{18}F-FDG PET/MRI for staging and restaging in paediatric oncology.

Pfluger T, **Melzer HI**, Mueller WP, Coppenrath E, Bartenstein P, Albert MH, Schmid I. Eur J Nucl Med Mol Imaging. 2012 Nov;39(11):1745-55.

In dieser Studie wurde der mögliche Zusatznutzen einer kombinierten ^{18}F-FDG-PET/MRT-Diagnostik im Vergleich zur solitären Bildgebungsmodalität in der pädiatrischen Onkologie untersucht. Die Fragestellung ergab sich aus der Problematik, dass sowohl die ^{18}F-FDG-PET als auch die MRT alleine häufig zu unzureichenden Aussagen in der Diagnostik pädiatrischer Krebserkrankungen führen. Während sich in der Erwachsenenonkologie die kombinierte Bildgebung bereits in Form des PET-CT-Scans etabliert hat, erfolgt die Anwendung der PET-CT in der Pädiatrie nur nach strenger Indikationsstellung [3], [11]. Die applizierte Strahlendosis der PET-CT-Untersuchung wird hauptsächlich durch das CT-Protokoll bestimmt [12]. Aufgrund der erhöhten Empfindlichkeit von Kindern gegenüber ionisierender Strahlung und des damit verbundenen höheren Risikos für strahleninduzierte Sekundärmalignome wird die PET-CT in der Pädiatrie zurückhaltend eingesetzt [13]. Demgegenüber ist die MRT zwar ein strahlungsfreies Verfahren, jedoch bestehen beim alleinigen Einsatz der MRT häufig Schwierigkeiten, sehr kleine Läsionen und Knochenmarksmetastasen bildmorphologisch darzustellen und zu identifizieren [14]. Zudem ist eine Unterscheidung zwischen vitalem Tumorgewebe und avitalen residualen Gewebeveränderungen nach Therapie nur eingeschränkt möglich, was vor allem zu Fehlinterpretationen im Follow-up führt [15]. Da die eingangs erwähnte applizierte Strahlendosis jedoch zum überwiegenden Teil durch das CT-Protokoll verursacht wird, erscheint der Einsatz der ^{18}F-FDG-PET bei Kindern prinzipiell hinsichtlich der damit verbundenen Risiken gerechtfertigt [12]. Um wie in der Erwachsenen-

onkologie die oben genannten methodenimmanenten Nachteile einer rein morphologischen Bildgebung auszugleichen, kommt bei Kindern somit die Kombination der strahlungsfreien MRT mit der ^{18}F-FDG-PET in Frage.

Um die diagnostische Wertigkeit der kombinierten Diagnostik mit ^{18}F-FDG-PET/MRT gegenüber den Einzelverfahren zu evaluieren, wurden 132 pädiatrische Patienten in die Studie eingeschlossen und insgesamt 813 bildmorphologische Läsionen in 270 Untersuchungspaaren untersucht. Zum Zeitpunkt der Untersuchung bestand bei jedem Patienten der Verdacht auf eine maligne Erkrankung oder der Patient wurde im Rahmen des Therapiemonitorings bei bestätigter onkologischer Erkrankung im Follow-up untersucht. Eine Vorselektion bezüglich der Tumorentitäten fand dabei nicht statt. Zunächst wurden in separater Analyse die ^{18}F-FDG-PET-Bilddaten und die MRT-Bilddaten ausgewertet. Anschließend erfolgte eine kombinierte Bildanalyse teilweise mithilfe einer Bildfusion. In der Datenauswertung wurden zum einen alle 813 malignitätsverdächtigen Läsionen einzeln beurteilt, und zum anderen erfolgte eine untersuchungsbezogene Bildbetrachtung der 270 Untersuchungspaare. Hierbei war die genaue Metastasenanzahl unerheblich, jeder Patient wurde zum Zeitpunkt der Untersuchung als positiv oder negativ für das Vorliegen einer Tumorerkrankung eingestuft.

In der Datenanalyse der Einzelläsionen betrug die Sensitivität der ^{18}F-FDG-PET 86 %, der MRT 94 % und der kombinierten ^{18}F-FDG-PET/MRT 97 %. Die Spezifität stellte sich für die ^{18}F-FDG-PET mit 85 %, für die MRT mit 38 % und für die kombinierte ^{18}F-FDG-PET/MRT mit 81 % dar. Somit konnte gezeigt werden, dass die kombinierte ^{18}F-FDG-PET/MRT-Diagnostik den Einzelverfahren hinsichtlich der Sensitivität überlegen ist. Folglich profitieren die Patienten von beiden Untersuchungsmodalitäten; die ^{18}F-FDG-PET ermöglicht ein gezieltes Staging mit Metastasensuche und die MRT dient vor allem der Darstellung der lokalen Tumorausdehnung, was zur Biopsie- oder Operationsplanung unerlässlich ist.

Dagegen war in der untersuchungsbezogenen Auswertung die MRT mit einer Sensitivität von 100 % in der Primärdiagnostik der kombinierten ^{18}F-FDG-PET/MRT (100 %) und der ^{18}F-FDG-PET (98 %) gleichwertig beziehungsweise überlegen. Als Konsequenz dieser Ergebnisse sollte bei Malignitätsverdacht zunächst eine MRT-Untersuchung zur Darstellung der lokalen Tumorausdehnung sowie zur Biopsie- und Operationsplanung erfolgen. Sofern eine bestätigte maligne Erkrankung mit Verdacht auf eine multilokuläre Ausdehnung vorliegt, sollte die Diagnostik im nächsten Schritt um eine ^{18}F-FDG-PET zum exakten Staging und zur Suche von auf den MRT-Aufnahmen nicht sichtbaren Metastasen ergänzt werden. Im Follow-up jedoch stellte sich die ^{18}F-FDG-PET als spezifischste Untersuchungsmodalität mit einer Spezifität von 81 % im Gegensatz zur MRT mit 30 % und der ^{18}F-FDG-PET/MRT mit 71 % dar. Somit ist im Follow-up die ^{18}F-FDG-PET die alleinig ausreichende Bildgebungsmethode. Jedoch empfiehlt sich im Falle eines ^{18}F-FDG-PET positiven Herdes mit

vermutetem Rezidiv oder Metastasen im Anschluss eine MRT-Untersuchung zur besseren morphologischen Übersicht und weiteren Therapieplanung. Allerdings sind einige Organsysteme wie zum Beispiel die Nieren und ableitenden Harnwege mit der ^{18}F-FDG-PET nur unzureichend beurteilbar. ^{18}F-FDG wird renal ausgeschieden und sammelt sich in der Harnblase an. Tumoren in diesen Arealen sind häufig nicht von der umgebenden Radiotraceransammlung zu unterscheiden. Bei vermuteter maligner Erkrankung in diesen Regionen ist deshalb das morphologische Korrelat der MRT sowohl in der Primärdiagnostik als auch im Follow-up unverzichtbar.

1.9 ^{18}F-FDG-PET verglichen mit ^{123}I-MIBG-Szintigraphie/SPECT

^{123}I-MIBG scintigraphy/SPECT versus ^{18}F-FDG PET in paediatric neuroblastoma.

Melzer HI, Coppenrath E, Schmid I, Albert MH, von Schweinitz D, Tudball C, Bartenstein P, Pfluger T. Eur J Nucl Med Mol Imaging. 2011 Sep;38(9):1648-58.

Die zweite dieser Arbeit zugrunde liegende Studie beschäftigt sich mit der Diagnostik peripherer neuroblastischer Tumoren. Neuroblastome sind embryonale Tumoren und entstehen entweder aus dem Nebennierenmark oder Ganglien des Grenzstrangs [16]. Zur Gruppe der peripheren neuroblastischen Tumoren gehören je nach Anteil der Stromakompontente die Neuroblastome, Ganglioneuroblastome und die Ganglioneurome. Je nach Differenzierungsgrad werden gut oder wenig differenzierte, reife oder unreife, sowie undifferenzierte Tumorzellen in der Histologie unterschieden [16]. Aufgrund ihres neuroektodermalen Ursprungs ist die Mehrzahl der Neuroblastome fähig, Katecholamine zu produzieren und zu verstoffwechseln [17]. Dies nutzt die nuklearmedizinische Bildgebung mit der ^{123}I-MIBG-Szintigraphie/SPECT, die heutzutage die bevorzugte Bildgebungsmodalität bei Verdacht auf ein Neuroblastom ist [18]. ^{123}I-MIBG wird als Noradrenalinanalogon in die Zelle aufgenommen und gespeichert [9]. Aufgrund noch ungeklärter Ursache verlieren jedoch ca. 8 % der Neuroblastome die Fähigkeit ^{123}I-MIBG anzureichern, wodurch falsch negative ^{123}I-MIBG-Szintigraphie/SPECT Befunde entstehen [19]. Die ^{123}I-MIBG-Szintigraphie/SPECT-Untersuchung ist für diese Untergruppe der Neuroblastompatienten in der Primärdiagnostik und im Follow-up daher nicht geeignet.
In dieser Studie wurde untersucht, ob bei Neuroblastompatienten mit negativer oder nicht aussagekräftiger ^{123}I-MIBG-Szintigraphie/SPECT die nachgeschaltete Untersuchung mit ^{18}F-FDG-PET einen diagnostischen Zusatznutzen bringt und deshalb generell empfohlen werden sollte. Dazu wurden 19 pädiatrische Patienten mit peripheren neuroblastischen Tumoren in die Studie eingeschlossen. Diese Patienten erhielten zunächst eine ^{123}I-MIBG-Szintigraphie/SPECT sowie im Abstand von wenigen Tagen eine ^{18}F-FDG-PET-Diagnostik. Insgesamt wurden 23 Untersuchungspaare ausgewertet und 58 Läsionen evaluiert. Es

zeigte sich, dass neuroblastische Tumoren, die kein oder nur sehr wenig ^{123}I-MIBG anreichern, in der ^{18}F-FDG-PET einen deutlichen Hypermetabolismus aufweisen können. Die Sensitivität der ^{123}I-MIBG-Szintigraphie/SPECT im Vergleich zur ^{18}F-FDG-PET für dieses Patientenkollektiv betrug 50 % zu 78 %, die Spezifität 75 % zu 92 %. In dieser Patientengruppe stellte sich die ^{18}F-FDG-PET damit sensitiver und spezifischer dar als die ^{123}I-MIBG-Szintigraphie/SPECT. Maligne Neuroblastomzellen, die die Fähigkeit zur ^{123}I-MIBG Aufnahme verloren haben, sind demzufolge mithilfe der ^{18}F-FDG-PET darstellbar und die nachgeschaltete ^{18}F-FDG-PET ist mit einem eindeutigen diagnostischen Zusatznutzen verbunden. Als Konsequenz dieser Ergebnisse wird folgender Diagnostikalgorithmus vorgeschlagen: Pädiatrische Patienten mit Verdacht auf Neuroblastom erhalten zunächst eine ^{123}I-MIBG-Szintigraphie/SPECT und eine MRT-Untersuchung. Zeigt sich eine Diskrepanz zwischen funktioneller und morphologischer Bildgebung oder den klinischen Befunden, wird als nächstes ergänzend eine ^{18}F-FDG-PET durchgeführt. Hat sich ein neuroblastischer Tumor als nicht ^{123}I-MIBG-affin erwiesen, so bietet sich die ^{18}F-FDG-PET als alleinige Bildgebungsmethode zur Vitalitätskontrolle im Follow-up an. Auf eine ^{123}I-MIBG-Szintigraphie/SPECT kann in diesem Fall verzichtet werden.

2. Zusammenfassung

Thema dieser Dissertation ist die multimodale Bildgebung in der pädiatrischen Onkologie. In beiden zugrunde liegenden publizierten Studien wird die Aussagekraft der ^{18}F-Fluordesoxyglukose Positronenemissionstomographie (^{18}F-FDG-PET) kombiniert mit einer weiteren Bildgebungsmodalität bei pädiatrisch-onkologischen Patienten evaluiert. Die ^{18}F-FDG-PET zählt zu den funktionellen Bildgebungsverfahren. Mithilfe radioaktiv markierter Glukose wird der Hypermetabolismus maligne entarteter Zellen dargestellt. Dies führt zur Visualisierung des Primärtumors, hilft bei der Metastasensuche und ermöglicht ein exaktes Tumorstaging.

In der ersten Studie wurde in einem hinsichtlich der Tumorentitäten nicht vorselektierten, onkologisch-pädiatrischen Patientenkollektiv die kombinierte ^{18}F-FDG-PET/MRT-Diagnostik mit den jeweiligen Einzelmodalitäten in der Erkennung maligner Läsionen verglichen. In der Primärdiagnostik stellte sich die kombinierte ^{18}F-FDG-PET/MRT-Bildgebung der alleinigen ^{18}F-FDG-PET- oder MRT-Diagnostik als überlegen heraus. Im Follow-up erwies sich die ^{18}F-FDG-PET aufgrund ihrer hohen Spezifität als geeignete alleinige Bildgebungsmodalität; eine weitere Untersuchung mittels MRT bringt im Falle einer negativen ^{18}F-FDG-PET keinen zusätzlichen diagnostischen Nutzen. Als Ausnahme gelten Tumoren des Urogenitaltraktes, die mittels ^{18}F-FDG-PET nicht sicher von unspezifischen Radiotraceransammlungen in den harnableitenden Wegen abgegrenzt werden können.

In der zweiten Studie wurde der Nutzen einer nachgeschalteten ^{18}F-FDG-PET-Bildgebung bei pädiatrischen Patienten mit peripheren neuroblastischen Tumoren untersucht, die in der Standarddiagnostik mittels ^{123}I-Metaiodbenzylguanidin (^{123}I-MIBG)-Szintigraphie/Single Photon Emission Computer Tomography (SPECT) keine aussagekräftigen Befunde aufzeigten. Dies ist in der täglichen Routinediagnostik bei ca. 8 % der Patienten mit Neuroblastom beziehungsweise peripheren neuroblastischen Tumoren der Fall. In dieser Studie konnte gezeigt werden, dass der unspezifische Radiotracer ^{18}F-FDG sich sehr gut in Neuroblastomen anreichert und somit hilfreich für die Tumor- und Metastasendarstellung und das Staging ist. Folglich sollte bei Verdacht auf ein Neuroblastom im Fall einer Diskrepanz zwischen ^{123}I-MIBG-Szintigraphie/SPECT, MRT und den klinischen Befunden eine ^{18}F-FDG-PET ergänzend erfolgen. Zur Verlaufskontrolle primär ^{123}I-MIBG-negativer neuroblastischer Tumoren stellte sich die ^{18}F-FDG-PET allein als suffiziente Bildgebungsmethode heraus.

Zusammenfassend erwies die ^{18}F-FDG-PET im Rahmen kombinierter Bildgebungsmodalitäten sowohl in der Primärdiagnostik als auch im Follow-up maligner Erkrankungen in der Pädiatrie als mitentscheidende funktionelle Untersuchungsmodalität.

3. Summary

The evaluation of multimodal imaging in paediatric oncology is the main theme of this thesis. Both published studies evaluate ^{18}F-fluorodesoxyglucose positron emission tomography (^{18}F-FDG-PET) combined with an additional imaging modality in paediatric oncological patients. ^{18}F-FDG-PET is a functional imaging modality, using radioactive glucose to demonstrate hypermetabolism in malignant transformed cells. Therefore, it enables the visualisation of the primary tumour, helps with the search for metastases, and leads to exact tumour staging.

The first study focuses on combined ^{18}F-FDG-PET/MR imaging in comparison to ^{18}F-FDG-PET or MR imaging alone for the detection of malignant lesions in a non-selected patient collective. In patients suffering from a variety of paediatric tumours, combined ^{18}F-FDG-PET/MR imaging proofed its utility in the primary diagnostic work-up. In the follow-up, ^{18}F-FDG-PET is recommended as single imaging modality due to its high specificity unless the malignancy is located in ^{18}F-FDG-PET inaccessible regions such as the urinary tract, where unspecific radiotracer accumulation hides malignant transformed tissue.

The focus of the second study is on ^{18}F-FDG-PET as a diagnostic tool in children with peripheral neuroblastic tumours. Neuroblastomas are commonly visualized on the ^{123}I-metaiodobenzylguanidine (^{123}I-MIBG)-scintigraphy/single photon emission computer tomography (SPECT). However, a subgroup of neuroblastomas fails to accumulate the specific radiotracer ^{123}I-MIBG. In this study, the non-specific radiotracer ^{18}F-FDG demonstrated a high affinity to neuroblastoma and helped detecting malignant disease. In case of a discrepancy between ^{123}I-MIBG scintigraphy/SPECT, MRI and clinical findings in patients with neuroblastic tumours, ^{18}F-FDG is recommended in the primary diagnostic work-up. In the follow-up of primary ^{123}I-MIBG negative neuroblastic tumours, ^{18}F-FDG-PET is sufficient as single imaging modality.

To sum up, in both studies, ^{18}F-FDG-PET combined with an additional imaging modality demonstrated to be indispensable in paediatric oncology for both the primary diagnostic work-up and the follow-up.

4. Literaturverzeichnis

[1] Connolly LP, Drubach LA, Ted TS. Applications of nuclear medicine in pediatric oncology. *Clin Nucl Med*. 2002;27(2):117-125.

[2] Smith MA, Seibel NL, Altekruse SF et al. Outcomes for children and adolescents with cancer: challenges for the twenty-first century. *J Clin Oncol*. 2010;28(15):2625-2634.

[3] Schiepers C, Dahlbom M. Molecular imaging in oncology: the acceptance of PET/CT and the emergence of MR/PET imaging. *Eur Radiol*. 2011;21(3):548-554.

[4] Fletcher JW, Djulbegovic B, Soares HP et al. Recommendations on the use of 18F-FDG PET in oncology. *J Nucl Med*. 2008;49(3):480-508.

[5] Reiser M, Kuhn F, Debus J. *Duale Reihe Radiologie*. Thieme Verlag; 2011.

[6] Zaidi H, Del GA. An outlook on future design of hybrid PET/MRI systems. *Med Phys*. 2011;38(10):5667-5689.

[7] Shulkin BL, Hutchinson RJ, Castle VP, Yanik GA, Shapiro B, Sisson JC. Neuroblastoma: positron emission tomography with 2-[fluorine-18]-fluoro-2-deoxy-D-glucose compared with metaiodobenzylguanidine scintigraphy. *Radiology*. 1996;199(3):743-750.

[8] Darge K, Jaramillo D, Siegel MJ. Whole-body MRI in children: current status and future applications. *Eur J Radiol*. 2008;68(2):289-298.

[9] Freitas JE. Adrenal cortical and medullary imaging. *Semin Nucl Med*. 1995;25(3):235-30.

[10] Voss SD. Pediatric oncology and the future of oncological imaging. *Pediatr Radiol*. 2011;41 Suppl 1:S172-S185.

[11] Mawlawi O, Townsend DW. Multimodality imaging: an update on PET/CT technology. *Eur J Nucl Med Mol Imaging*. 2009;36 Suppl 1:S15-S29.

[12] Pichler BJ, Kolb A, Nagele T, Schlemmer HP. PET/MRI: paving the way for the next generation of clinical multimodality imaging applications. *J Nucl Med*. 2010;51(3):333-336.

[13] Kleinerman RA. Cancer risks following diagnostic and therapeutic radiation exposure in children. *Pediatr Radiol*. 2006;36 Suppl 2:121-125.

[14] Daldrup-Link HE, Franzius C, Link TM et al. Whole-body MR imaging for detection of bone metastases in children and young adults: comparison with skeletal scintigraphy and FDG PET. *AJR Am J Roentgenol*. 2001;177(1):229-236.

[15] Ratib O, Beyer T. Whole-body hybrid PET/MRI: ready for clinical use? *Eur J Nucl Med Mol Imaging*. 2011;38(6):992-995.

[16] Shimada H, Ambros IM, Dehner LP, Hata J, Joshi VV, Roald B. Terminology and morphologic criteria of neuroblastic tumors: recommendations by the International Neuroblastoma Pathology Committee. *Cancer*. 1999;86(2):349-363.

[17] Strenger V, Kerbl R, Dornbusch HJ et al. Diagnostic and prognostic impact of urinary catecholamines in neuroblastoma patients. *Pediatr Blood Cancer*. 2007;48(5):504-509.

[18] Vik TA, Pfluger T, Kadota R et al. (123)I-mIBG scintigraphy in patients with known or suspected neuroblastoma: Results from a prospective multicenter trial. *Pediatr Blood Cancer*. 2009;52(7):784-790.

[19] Biasotti S, Garaventa A, Villavecchia GP, Cabria M, Nantron M, De BB. False-negative metaiodobenzylguanidine scintigraphy at diagnosis of neuroblastoma. *Med Pediatr Oncol*. 2000;35(2):153-155.

5. Danksagung

Für die freundliche Bereitstellung des Themas dieser Arbeit danke ich Herrn Professor Dr. med. Peter Bartenstein, Direktor und Lehrstuhlinhaber des Instituts für Nuklearmedizin der Ludwig-Maximilians Universität München.

Bei meinem persönlichen Betreuer, Herrn PD Dr. Thomas Pfluger möchte ich mich für die intensive Betreuung während meiner Promotionsarbeit sowie für die Hilfe beim Verfassen der Publikationen ganz besonders und herzlich bedanken.

Für kritische Anmerkungen und Unterstützung bedanke ich mich bei meinen Eltern Frau Dr. Susanne Pfuhl-Melzer und Herrn Dr. Karl-Heinz Melzer, sowie bei meinem Bruder Adrian Melzer. Besonderer Dank gilt auch meinem Freund Dr. Nicolas Thornton.

6. Lebenslauf

Die Seiten 16 und 17 (Lebenslauf) enthalten persönliche Daten. Sie sind deshalb nicht Bestandteil der Pflichtexemplare und der Online-Veröffentlichung.

Die Seiten 16 und 17 (Lebenslauf) enthalten persönliche Daten. Sie sind deshalb nicht Bestandteil der Pflichtexemplare und der Online-Veröffentlichung.

7. Originalarbeiten

Eur J Nucl Med Mol Imaging (2012) 39:1745–1755
DOI 10.1007/s00259-012-2228-3

ORIGINAL ARTICLE

Diagnostic value of combined ^{18}F-FDG PET/MRI for staging and restaging in paediatric oncology

Thomas Pfluger · Henriette I. Melzer · Wolfgang P. Mueller · Eva Coppenrath · Peter Bartenstein · Michael H. Albert · Irene Schmid

Received: 16 May 2012 / Accepted: 9 August 2012 / Published online: 28 August 2012

Abstract
Purpose The present study compares the diagnostic value of ^{18}F-fluorodeoxyglucose (FDG) positron emission tomography (PET) and MRI to combined/registered ^{18}F-FDG PET/MRI for staging and restaging in paediatric oncology.
Methods Over 8 years and 2 months, 270 ^{18}F-FDG PET and 270 MRI examinations (mean interval 5 days) were performed in 132 patients with proven (n=117) or suspected (n=15) malignant disease: solid tumours (n=64), systemic malignancy (n=53) and benign disease (n=15). A total of 259 suspected tumour lesions were analysed retrospectively during primary diagnosis and 554 lesions during follow-up. Image analysis was performed separately on each modality, followed by analysis of combined and registered ^{18}F-FDG PET/MRI imaging.
Results A total of 813 lesions were evaluated and confirmed by histopathology (n=158) and/or imaging follow-up (n=655) after 6 months. In the separate analysis of ^{18}F-FDG PET and MRI, sensitivity was 86 %/94 % and specificity 85 %/38 %. Combined/registered ^{18}F-FDG PET/MRI led to a sensitivity of 97 %/97 % and specificity of 81 %/82 %. False-positive results (^{18}F-FDG PET n=69, MRI n=281, combined ^{18}F-FDG PET/MRI n=85, registered ^{18}F-FDG PET/MRI n=80) were due to physiological uptake or post-therapeutic changes. False-negative results (^{18}F-FDG PET n=50, MRI n=20, combined ^{18}F-FDG PET/MRI n=11, registered ^{18}F-FDG PET/MRI n=11) were based on low uptake or minimal morphological changes. Examination-based evaluation during follow-up showed a sensitivity/specificity of 91 %/81 % for ^{18}F-FDG PET, 93 %/30 % for MRI and 96 %/72 % for combined ^{18}F-FDG PET/MRI.
Conclusion For the detection of single tumour lesions, registered ^{18}F-FDG PET/MRI proved to be the methodology of choice for adequate tumour staging. In the examination-based evaluation, MRI alone performed better than ^{18}F-FDG PET and combined/registered imaging during primary diagnosis. At follow-up, however, the examination-based evaluation demonstrated a superiority of ^{18}F-FDG PET alone.

Keywords Paediatric oncology · ^{18}F-FDG PET · MRI · Combined/registered image analysis

T. Pfluger · H. I. Melzer (✉) · W. P. Mueller · P. Bartenstein
Department of Nuclear Medicine,
Ludwig Maximilians University of Munich,
Ziemssenstraße 1,
80336 Munich, Germany
e-mail: melzer.henriette@yahoo.de

E. Coppenrath
Department of Radiology,
Ludwig Maximilians University of Munich,
Munich, Germany

M. H. Albert · I. Schmid
Department of Paediatric Oncology/Haematology,
Ludwig Maximilians University of Munich,
Munich, Germany

Introduction

From 1975 to 2006 the combined mortality rate of all malignant childhood cancers declined by more than 50 % [1]. Early detection of disease or relapse, staging of the malignancy and therapy monitoring are important for patient management and prognosis [2]. In 1998, combined morphological and functional imaging was implemented in the positron emission tomography (PET)/CT scanner [3]. PET with ^{18}F-fluorodeoxyglucose (FDG) proved its utility in adult oncology, but its inability to provide anatomical information displays a significant weakness [4, 5]. Combination of the high sensitivity and specificity of ^{18}F-FDG PET with

the high anatomical resolution of CT improves diagnostic accuracy [6, 7]. Currently, PET/CT is a major diagnostic tool in oncology [2, 8]. However, an important disadvantage of a CT scan is the exposure to ionizing radiation [9]. In paediatric patients, radiation exposure is of particular concern due to an increased susceptibility of children towards secondary malignancies induced by radiation compared to adults [10]. The main radiation dose of PET/CT is often due to the CT protocol with a range of 1.3–18.6 mSv for a CT scan [9, 11]. MRI offers an alternative morphological imaging approach avoiding additional radiation exposure [12, 13]. Since it provides excellent soft tissue contrast and since fast imaging sequences including whole-body imaging capabilities are available, ideas of integrated PET/MRI have emerged [14, 15]. The first simultaneous PET/MR images have been acquired of the human brain and body [16, 17]. The aim of this retrospective study was to determine the diagnostic value of combined and registered image analysis of ^{18}F-FDG PET and MRI for staging and restaging in paediatric oncology.

Materials and methods

Patients

Over a time period of 8 years and 2 months, 270 MRI and 270 ^{18}F-FDG PET examinations were performed in 132 paediatric patients (77 male and 55 female, mean age 11 years and 1 month, age range 9 months–18 years and 3 months) and were analysed retrospectively. All patients had suspected (n=15) or pathologically proven (n=117) malignant disease (Table 1). For all patients, written informed consent was available. Of the patients, 33 were examined for primary diagnosis, 56 for follow-up and 43 for both settings. A total of 76 combined MRI and ^{18}F-FDG PET studies were performed for initial staging and 194 during follow-up. Follow-up scans were performed in a free interval of at least 4 weeks after tumour-specific therapy or—for benign disorders—after an appropriate watch and wait period. Inclusion criteria were suspected malignant disease and a maximum time frame of 30 days (mean time interval 5 days, range 0–30 days) between the MRI and the ^{18}F-FDG PET examinations. Patients were excluded if there had been any tumour-specific therapy between ^{18}F-FDG PET and the MRI scan. For each lesion, histopathology and/or imaging follow-up data after a minimal time period of 6 months had to be available.

Acquisition protocol

^{18}F-FDG PET scans were performed with an Allegro PET scanner (Philips Medical Systems, Hamburg, Germany). All patients fasted for at least 4 h and blood glucose level was examined for deviation from normal level prior to ^{18}F-FDG PET imaging. One hour before scanning, ^{18}F-FDG with a dosage according to the body weight and the guidelines of the European Association of Nuclear Medicine (EANM) [18] (range 30–200 MBq, mean 125 MBq) was injected intravenously, and the patient was instructed to rest until the beginning of the examination. ^{18}F-FDG PET was performed using three to ten bed positions (depending on the size of patients) with a 2-min acquisition time per bed position. Images were attenuation corrected using transmission scans obtained with a ^{137}Cs source. Data acquisition was done in three-dimensional mode using a row action maximum likelihood algorithm (3-D RAMLA). The examination field of view (FOV) was of the whole body. ^{18}F-FDG PET images were reviewed on a HERMES workstation (Nuclear Diagnostics, Hägersten, Sweden).

MRI was performed with a 1.5 T scanner (Magnetom Vision, Siemens, Erlangen, Germany). The FOV included the region suspected of tumour affection. Lesions were included for evaluation only if they were within the FOV of ^{18}F-FDG PET as well as MRI. Head or body array coils were used according to the size of the patient. Axial, coronal or sagittal spin-echo or fast spin-echo T1- and T2-weighted images and short τ inversion recovery (STIR) images were obtained. The slice thickness ranged from 3 to 6 mm. In addition, gadopentetate dimeglumine (Magnevist, Schering, Berlin, Germany) was injected intravenously (0.2 ml/kg of body weight) to assess contrast enhancement of suspected lesions on T1-weighted sequences. Sedation was necessary for ^{18}F-FDG PET in nearly all children aged 2 years or younger (n=9), for MRI in nearly all children aged 4 years or younger (n=17) or if patients were uncooperative (n=13).

Image analysis

Lesion-based image analysis was performed by reviewing the images of both modalities. A lesion was included if it was considered positive for tumour involvement either on ^{18}F-FDG PET or MRI. Individual data analyses of both modalities were performed by two independent observers with long-term experience (>5 years) with paediatric ^{18}F-FDG PET as well as paediatric MRI diagnostics. Analysis was obtained with knowledge of clinical data and laboratory results, but without knowledge of the findings of the other imaging modality. To determine whether regression or disappearance of lesions was evident on follow-up examinations, observers needed to know the findings from the previous examination of the same modality. A total of 813 suspicious lesions were evaluated. There were 67 patients who had several examination pairs (43 patients primary diagnosis and follow-up—24 several follow-up examinations); hence, their lesions were reanalysed in at least 1 (or up to 5) follow-up examination. On ^{18}F-FDG PET, a lesion

Table 1 Confirmed diagnoses in 813 lesions suspected of tumour affection at primary diagnosis and follow-up

Final diagnosis	Patients (n=132)	Lesions (n=813)	Size (cm)	PET_{pos} PD (n=217)	PD SUV_{max}	PET_{pos} F/U (n=162)	F/U SUV_{max}
Systemic malignant tumours							
Acute lymphatic leukaemia	2	6	2.1	1	11.6	5	5.1
Burkitt's lymphoma	4	9	1.6	1	12.2	4	3.5
Hodgkin's lymphoma	33	366	2.6	96	5.4	50	3.6
Non-Hodgkin's lymphoma	13	88	1.7	38	7.2	3	5.2
Langerhans cell histiocytosis	1	3	1.8	0	–	1	0.7
Solid malignant tumours							
Adrenal gland carcinoma	2	6	1.9	1	4.1	3	3.6
Carcinoma of the salivary gland	1	2	0.9	0	–	0	–
Carcinoma of the small intestine	1	8	0.9	0	–	3	1.5
Germ cell tumour/yolk sac tumour	4	18	2.8	1	2.8	9	2.9
Hepatoblastoma/hepatic cell carcinoma	3	6	2.6	0	–	6	2.5
Malignant schwannoma	1	2	1.6	0	–	2	1.2
Neuroblastoma	6	60	3.9	12	2.6	11	2.6
Neuroendocrine neoplasm	1	6	1.2	3	4.6	0	–
Pancreatic carcinoma	1	8	1.4	0	–	0	–
Primitive neuroectodermal tumour	4	27	2.3	0	–	21	2.5
Pneumoblastoma	1	1	2.0	0	–	1	2.7
Renal cell carcinoma/Wilms' tumour	2	8	3.4	2	4.2	2	2.2
Rhabdomyosarcoma	15	77	3.4	22	3.3	16	1.9
Sarcoma of soft tissue and bone	21	81	3.2	22	4.5	22	2.7
Thyroid carcinoma	1	1	1.1	0	–	1	2.6
Benign tumours							
Adrenal gland adenoma	1	1	1.8	0	–	0	–
Ganglioneuroma	3	4	2.5	1	1.6	0	–
Inflammatory pseudotumour	1	2	1.3	2	4.2	0	–
Lipoblastoma	1	1	1.7	0	–	0	–
Myxoid tumour	1	1	1.4	0	–	0	–
Neurofibromatosis	1	4	1.7	4	3.1	0	–
Inflammatory and lymphoproliferative disease							
Autoinflammatory syndrome	1	1	1.2	1	6.8	0	–
Chronic granulomatosis	1	2	1.6	2	4.3	0	–
Common variable immune deficiency	1	3	1.2	3	4.0	0	–
Inflammatory lymph nodes	1	4	1.5	2	2.4	0	–
Post-transplant lymphoproliferative disorder	1	5	1.2	1	3.9	2	4.4
Ossifying myositis	1	1	1.4	1	2.9	0	–
Sarcoidosis	1	1	1.3	1	2.3	0	–

PD primary diagnosis, *F/U* follow-up

was judged positive if it showed a non-physiological glucose metabolism with a maximum standardized uptake value (SUV_{max}) higher than that of the patient's normal right liver lobe. The SUV is used in PET imaging for (semi-)quantitative analysis of ^{18}F-FDG uptake. The SUV is calculated over a region of interest at time points t as the ratio of tissue radioactivity concentration (MBq/kg) at time t and injected dose (MBq) at the time of injection divided by body weight (kg) [19]. For determination of SUV_{max}, maximum tissue radioactivity concentration of the region of interest was taken. On MRI scans, morphologically suspicious lesions with increased contrast enhancement and/or oedematous changes were judged positive. For observers to reach a decision on lesions with discrepant results on both modalities, a diagnostic confidence score of three levels was established for each modality: 1=both observers were uncertain

about a positive or negative finding, 2=one observer was uncertain and one observer was certain and 3=both observers were certain. The diagnostic confidence score was assigned to each lesion on ^{18}F-FDG PET and on the MRI scan separately. Combined assessment of both modalities was based on the diagnostic confidence score of separate modalities and performed by the same two observers. In case of discrepancies, the finding of the modality with the higher diagnostic confidence level was used. If both modalities were discrepant and revealed the same score value, the lesion was judged positive. Combined image analysis was done by reviewing both data sets (^{18}F-FDG PET and MRI) side by side on one workstation, however, without any kind of image synchronization. For analysis of registered image data sets, a computer-assisted interactive matching method was used, where ^{18}F-FDG PET and MRI data sets were superimposed manually on a HERMES workstation (Nuclear Diagnostics, Hägersten, Sweden) in all three orientations. As a result, spatially synchronized images could be reviewed side by side and/or in an image fusion mode on one workstation. In combined and registered image analysis, a lesion was judged positive if the area of increased ^{18}F-FDG uptake was concordant with a morphologically detectable lesion on MRI and did not correspond to physiological structures. In the examination-related assessment, the whole examination was judged positive with respect to vital tumour tissue if at least one of the assessed lesions was positive.

Standard of reference

The standard of reference was established by histopathological findings of the lesions (n=158) or imaging follow-up controls (n=655) after a minimal time period of 6 months (^{18}F-FDG PET and MRI: n=283, MRI: n=224, ^{18}F-FDG PET: n=148). A lesion was classified as either “false-positive” or “true-negative” if it disappeared without any tumour-specific therapy during the observation period or if it turned out to be an obvious physiological structure or uptake. A non-physiological structure was classified as either “true-positive” or “false-negative” if it persisted or progressed during follow-up or showed an objective regression under specific therapy.

Statistical analysis

The diagnostic techniques were compared in terms of sensitivity and specificity based on true-positive, true-negative, false-positive and false-negative rates. The positive likelihood ratio was calculated for each modality. Sensitivity and specificity of two diagnostic techniques were compared using McNemar’s chi-square test. The p values were calculated two-sided, and $p<0.05$ was indicative of significance. The analysis was performed using the Statistical Package for the Social Sciences (SPSS, version 15.0, Chicago, IL, USA).

Results

Table 1 summarizes the distribution of the different tumour entities, the morphological lesion diameter and the SUV_{max}. Size and SUV_{max} of every single lesion were determined—in each row a mean diameter (in cm) and a mean SUV_{max} are given for the respective group of disease. Findings of primary diagnosis and follow-up are presented in Tables 2 and 3.

Lesion-based analysis

Of 813 lesions, 360 (44.3 %) proved to be vital tumour tissue. In the analysis of all lesions, ^{18}F-FDG PET, MRI, combined ^{18}F-FDG PET/MRI and registered ^{18}F-FDG PET/MRI resulted in a sensitivity of 86 %/94 %/97 %/97 % and in a specificity of 85 %/38 %/81 %/82 %. As there were only a few true-negative findings at primary diagnosis, specificity was not calculated in this context. At follow-up, the sensitivity of ^{18}F-FDG PET alone was significantly lower than the sensitivity of MRI ($p<0.001$) or combined/registered ^{18}F-FDG PET/MRI ($p<0.001$ for each pair). Follow-up specificity of MRI was significantly lower compared to the other diagnostic techniques ($p<0.001$ for each pair). In the assessment of all 813 lesions, ^{18}F-FDG PET classified 310 of 360 lesions as positive and 384 of 453 as negative for vital tumour involvement. The mean diagnostic confidence score was 2.5. Sources of false-positive and false-negative findings are shown in Table 4. In the assessment of all 813 lesions, MRI classified 340 of 360 lesions as positive and 172 of 453 as negative for vital tumour involvement. The mean diagnostic confidence score was 1.9. In the assessment of all 813 lesions, combined ^{18}F-FDG PET/MRI analysis classified 349 of 360 lesions as positive and 368 of 453 as negative and registered ^{18}F-FDG PET/MRI analysis 349 of 360 lesions as positive and 373 of 453 as negative for vital tumour involvement. ^{18}F-FDG PET and MRI resulted in discrepant findings in 326 lesions. ^{18}F-FDG PET was incorrect in 72 and MRI in 254 lesions.

Examination-based analysis

For a total of 270 scans, vital tumour was proven in 140 (51.8 %) examinations. Again, due to the low number of true-negative findings, specificity was not calculated for primary diagnosis. In disease follow-up, specificity of ^{18}F-FDG PET was significantly higher than specificity of MRI ($p<0.001$), combined ^{18}F-FDG PET/MRI ($p=0.008$) or

Table 2 Imaging findings of lesion-based analysis in primary diagnosis (n=259) and follow-up (n=554)

Findings	^{18}F-FDG PET		MRI		^{18}F-FDG PET/MRI image combination		^{18}F-FDG PET/MRI image registration	
	PD	F/U	PD	F/U	PD	F/U	PD	F/U
True-positive	197	113	201	139	215	134	215	134
True-negative	24	360	8	164	19	349	19	354
False-positive	20	49	36	245	25	60	25	55
False-negative	18	32	14	6	0	11	0	11
Sensitivity (%)	92	78	93	96	100	92	100	92
Specificity (%)	–	88	–	40	–	85	–	87
Pos. likelihood ratio	–	6.5	–	1.6	–	6.1	–	7.1

PD primary diagnosis, *F/U* follow-up examination

registered ^{18}F-FDG PET/MRI (p=0.019). Specificity of MRI was significantly lower than specificity of combined or registered ^{18}F-FDG PET/MRI (p<0.001 for each pair). The differences in sensitivity were not significant for all pairs in primary diagnosis and follow-up. Due to the higher diagnostic confidence score, all 11 false-positive scans from ^{18}F-FDG PET remained on combined imaging in primary diagnosis, although MRI could identify two suspicious lesions as physiological uptake. There was no difference between combined and registered ^{18}F-FDG PET/MRI analysis in primary diagnosis. In one patient with rhabdomyosarcoma, combined and registered ^{18}F-FDG PET/MRI led to the detection of the primary tumour, which was not identifiable on ^{18}F-FDG PET alone, and therefore influenced tumour staging. At follow-up, only combined and registered ^{18}F-FDG PET/MRI allowed correct tumour staging in eight patients. Combined and registered imaging could correct four false-negative ^{18}F-FDG PET and four false-negative MRI examinations. Those four false-negative findings on ^{18}F-FDG PET were due to lesions next to highly metabolic physiological structures and due to movement artefacts. In the examination-based analysis, there was no case where the only relevant tumour lesion was outside the FOV of MRI and only detectable with ^{18}F-FDG PET.

Discussion

As ^{18}F-FDG PET and MRI represent the most powerful functional and morphological imaging modalities in paediatric oncology nowadays, it is important to evaluate if a combined ^{18}F-FDG PET/MRI approach adds significant information to the use of separate imaging modalities during primary diagnosis and follow-up.

Lesion-based analysis

In our study, a special strength of ^{18}F-FDG PET was its sensitivity of more than 90 % during primary diagnosis and a specificity of more than 85 % during follow-up. These results confirm that ^{18}F-FDG PET is an important imaging modality in paediatric oncology. It influences therapeutic decisions and produces results comparable to adult oncology [20]. As reported in the literature, a source of false-positive findings is represented by physiological ^{18}F-FDG uptake in ureters, bowel, lymphatic tissue, thymus, brown fat and muscle [4] (Table 4, Fig. 1). In paediatric lymphoma patients, differentiation between a mediastinal mass and physiological thymic or increased post-therapeutic uptake is required [21]. In our setting, SUV_{max} was not an

Table 3 Imaging findings of examination-based analysis in primary diagnosis (n=76) and follow-up (n=194)

Findings	^{18}F-FDG PET		MRI		^{18}F-FDG PET/MRI image combination		^{18}F-FDG PET/MRI image registration	
	PD	F/U	PD	F/U	PD	F/U	PD	F/U
True-positive	63	69	64	71	64	73	64	73
True-negative	1	96	3	35	1	84	1	85
False-positive	11	22	9	83	11	34	11	33
False-negative	1	7	0	5	0	3	0	3
Sensitivity (%)	98	91	100	93	100	96	100	96
Specificity (%)	-	81	-	30	-	71	-	72
Pos. likelihood ratio	-	4.8	-	1.3	-	3.3	-	3.4

PD primary diagnosis, *F/U* follow-up examination

Table 4 Lesion-based analysis: source of false-positive and false-negative findings

Findings	Source	^{18}F-FDG PET		MRI		Comb. ^{18}F-FDG PET/MRI		Reg. ^{18}F-FDG PET/MRI	
		PD	F/U	PD	F/U	PD	F/U	PD	F/U
False-positive	Total	20	49	36	245	25	60	25	55
	Benign tumour	2	–	2	6	2	4	2	4
	Inflammatory tissue	12	16	32	31	19	18	19	19
	Physiological uptake/physiological structure	6	9	2	2	4	5	4	5
	Post-therapeutic changes/bone marrow oedema	–	24	–	206	–	33	–	27
False-negative	Total	18	32	14	6	0	11	0	11
	Low metabolic rate limited size	7	13	9	4	–	8	–	8
	Physiological uptake urinary tract	11	19	–	–	–	3	–	3
	Reactive soft tissue changes	–	–	5	2	–	–	–	–

PD primary diagnosis, *F/U* follow-up examination

appropriate parameter to discriminate between benign and malignant lesions. There was a large overlap especially between malignant and inflammatory lesions, which complicates lesion identification on ^{18}F-FDG PET (Table 1). A ganglioneuroma lesion showed increased ^{18}F-FDG uptake although ganglioneuroma is classified as benign [22]. Benign bone tumours can reach an SUV_{max} up to 3.5 [23], and malignant bone/bone marrow lesions normally range from 1.2 to 7.5 [24]. In inflammatory or irradiated tissue, an SUV_{max}>2.5 can frequently be found [25, 26] (Fig. 2). Granulocytes and mononuclear cells use glucose as an energy source during their metabolic burst [27]. Due to the immunocompromising effect of cytotoxic chemotherapy, infectious disease commonly occurs during or after chemotherapy [28]. In our study, the majority of false-positive findings were caused by post-therapeutic or inflammatory changes (Table 4). In false-negative findings, the tumour lesions could not be differentiated from surrounding healthy tissue with physiological uptake due to either limited size of the lesion or lesion site in structures with high physiological ^{18}F-FDG accumulation (Fig. 3). Furthermore, malignant tumours do not always accumulate ^{18}F-FDG: a low metabolic rate leads to weak uptake [4]. In addition, ^{18}F-FDG PET missed 2 of 11 intrapulmonary lesions. A known weakness of ^{18}F-FDG PET is its restricted spatial resolution of 4–10 mm in commercial scanners [4]: small nodular metastases are commonly missed and with ^{18}F-FDG PET/CT the sensitivity for the detection of malignant lesions of paediatric primary bone tumours is lower compared to conventional imaging [29]. However, the SUV_{max} evaluation of pulmonary lesions is important for the prediction of response to chemotherapy [29].

At primary diagnosis, MRI demonstrated a sensitivity of more than 90 %, which was comparable to the sensitivity of ^{18}F-FDG PET. At follow-up, MRI presented a high sensitivity but at the same time a significantly lower specificity when compared to ^{18}F-FDG PET, combined or registered ^{18}F-FDG PET/MRI (p<0.001 for each pair). MRI studies provide a diversity of diagnostic information regarding the

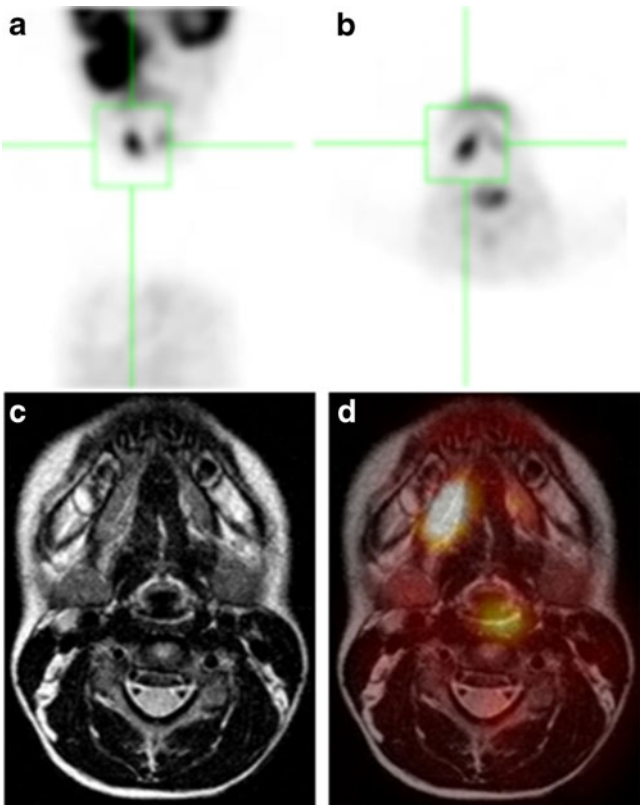

Fig. 1 A 5.5-year-old girl with rhabdomyosarcoma—false-positive on ^{18}F-FDG PET. At primary diagnosis, ^{18}F-FDG PET (**a**, **b**) shows an increased uptake in the submandibular region; a lymph node metastasis of the rhabdomyosarcoma was suspected. On the MRI (**c** T2-weighted sequence, **d** image fusion), no morphological changes are seen in this location. Therefore, the uptake corresponds to physiological muscle activity. During follow-up, the lesions disappeared on ^{18}F-FDG PET. The retromandibular primary tumour with its growth through the skull base is seen on ^{18}F-FDG PET (**a**)

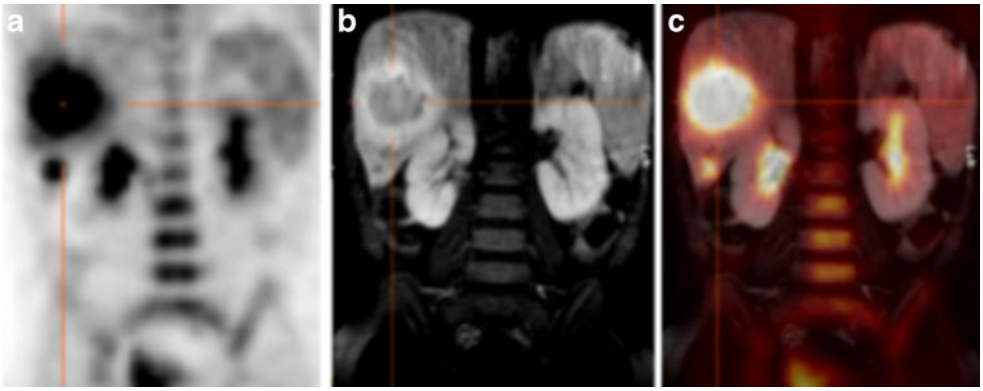

Fig. 2 A 4-year-old-boy with abdominal pain—false-positive on ^{18}F-FDG PET/MRI. During primary diagnosis, ^{18}F-FDG PET (**a**) shows increased uptake in wo intrahepatic lesions. MRI (**b** fat-suppressed T1-weighted sequence after contrast application) and registered images (**c**) demonstrate a contrast-enhancing necrotic mass. A malignant tumour of the liver could not be excluded. Biopsy showed an intrahepatic abscess

exact anatomical tumour site, tumour composition, soft tissue analysis and tissue characterization [30]. Therefore, MRI is important in the primary diagnostic workup to correctly assess the exact tumour and biopsy site for adequate therapy planning [31]. MRI showed difficulties in identifying viable bone/bone marrow tumour lesions due to limited morphological size and/or soft tissue changes at the time of scanning. False-positive findings were mostly caused by nonspecific inflammatory lymph node enlargement or infectious tissue changes (Table 4) [12, 32]. At follow-up, a major weakness of MRI was its low specificity—post-therapeutic changes like persisting bone marrow oedema (Fig. 4), necrotic tissue, contrast enhancement in successfully treated lesions and the fact that bone marrow appearance in children varies with age favoured the misinterpretation [12, 32]. Among lymphoma patients, Baba et al. demonstrated difficulties in distinguishing between vital tumour tissue and residual mass composed of necrosis or fibrosis on morphological imaging [33]. In our study, with many lymphoma patients, lymph node enlargement without active tumour was regularly seen on a post-therapeutic MRI scan. Few false-negative findings occurred when tumour involvement was missed because of small morphological size or recurrent disease in a post-surgical setting. Due to its low specificity, MRI is not sufficient as a single imaging modality in the follow-up.

At primary diagnosis, combined and registered image analysis of ^{18}F-FDG PET/MRI did not miss any tumour lesion and increased sensitivity to 100 %. ^{18}F-FDG PET/MRI especially proved its utility in the correct characterization of bone/bone marrow lesions. For the initial detection of skeletal metastases, Daldrup-Link et al. compared whole-body MRI to ^{18}F-FDG PET and bone scintigraphy in children and young adults: ^{18}F-FDG PET was the most sensitive imaging method [34]. Using combined and registered image analysis of ^{18}F-FDG PET/MRI no bone/bone marrow lesion was missed. In cases where physiological structures could not be distinguished from tumour tissue on ^{18}F-FDG PET, the high spatial resolution and soft tissue contrast of the MRI helped to outline the anatomical structure. In the follow-up, the sensitivity of combined and registered ^{18}F-FDG PET/MRI imaging was significantly lower than that of MRI alone in the lesion-based analysis ($p<0.001$ for each pair). This was due to our diagnostic confidence score, where lesions without any evidence of tumour involvement were assigned to a score value of 3. Therefore, in some of

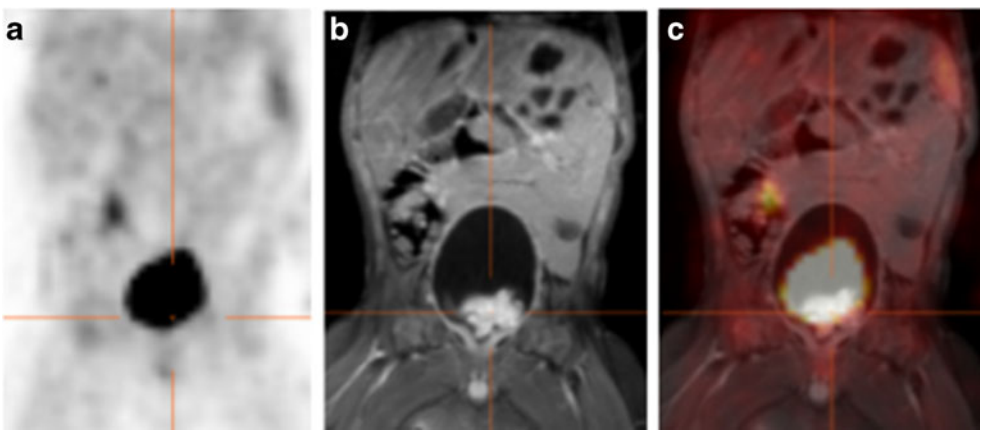

Fig. 3 A 1.5-year-old boy with rhabdomyosarcoma of the urinary bladder—false-negative on ^{18}F-FDG PET. The lesion in the bladder is not visible on ^{18}F-FDG PET (**a**) due to radiotracer accumulation in the urinary bladder. Fat-suppressed T1-weighted MRI after contrast application (**b**) shows an intravesical tumour. On the registered image (**c**) the disconcordant location of the bladder is due to different filling at the time of examination

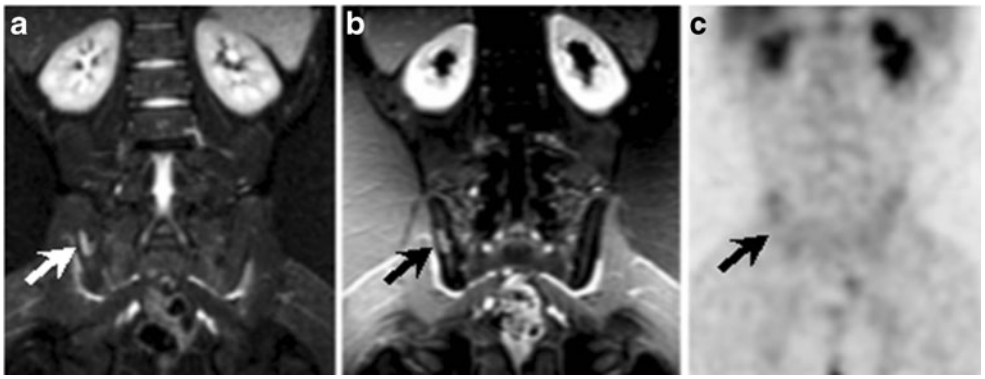

Fig. 4 A 9.5-year-old boy with Hodgkin's lymphoma—false-positive on MRI. At follow-up, MRI (**a** T2-weighted STIR, **b** T1-weighted sequence after contrast application) shows residual bone marrow oedema in the right iliac bone after chemotherapy (*arrow*). ^{18}F-FDG PET (**c**) and follow-up examinations confirmed disease remission

our cases with a discrepancy between ^{18}F-FDG PET and MRI, the false-negative ^{18}F-FDG PET finding overruled the true-positive MRI finding. With combined and registered imaging, the majority of false-positive findings in bone/bone marrow and in lymph nodes on MRI could be identified as post-therapeutic changes in successfully treated tumour lesions. With image registration, five false-positive findings could be adjusted in contrast to combined image analysis alone (Fig. 5). Positive likelihood ratios of ^{18}F-FDG PET, combined and registered ^{18}F-FDG PET/MRI further indicate a moderate improvement in post test probability in follow-up if positive. In our study, ^{18}F-FDG PET alone, combined and registered ^{18}F-FDG PET/MRI had higher specificities than MRI alone.

Examination-based analysis

In the examination-based analysis, at primary diagnosis, 11 examinations rated as false-positive remained even when using combined and registered imaging. The patients mainly suffered from inflammatory disease (Fig. 2). In these cases, tumour involvement has to be ruled out by histopathological analysis. Therefore, additional ^{18}F-FDG PET was not helpful for tumour detection and differentiation during primary diagnosis in our patient cohort. At the follow-up, ^{18}F-FDG PET resulted in seven false-negative scans due to a lesion location next to or in the urinary bladder, movement artefacts and a lung metastasis. In the literature, difficulties in evaluating the pelvis on ^{18}F-FDG PET due to the radiotracer

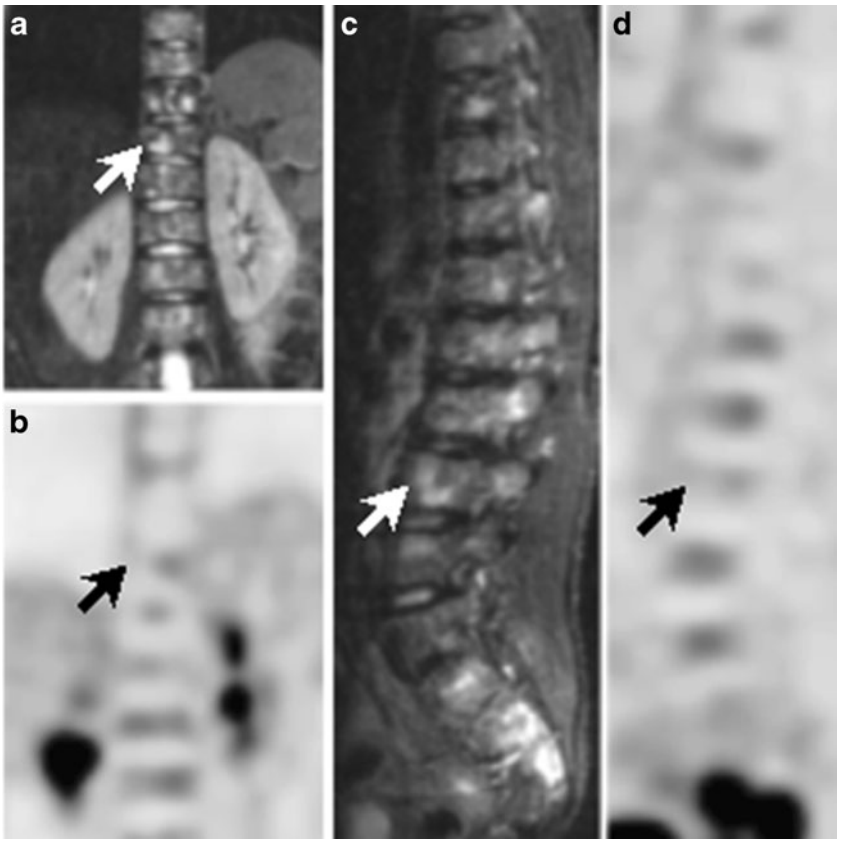

Fig. 5 A 10-year-old boy with metastasized Ewing sarcoma—false-positive on ^{18}F-FDG PET and MRI and true-negative on registered ^{18}F-FDG PET/MRI. At follow-up, MRI (**a**, **c** T2-weighted STIR) shows, among other things, increased signal in the 10th thoracic and 4th lumbar vertebral bodies. On the ^{18}F-FDG PET (**b**, **d**) multiple foci of increased ^{18}F-FDG uptake are found in the spine. Both modalities alone led to the suspicion of multiple vital metastases in the spine. However, on combined imaging after image registration, the areas of bone marrow oedema on MRI correspond to photopenic defects on ^{18}F-FDG PET, thereby proving inactivity of the respective lesions. This true-negative finding was confirmed at follow-up after 6 months, when the patient was in disease remission

accumulation in the urinary bladder have been reported by Mody et al. [35]. In case of obvious movement artefacts, morphological image correlation is recommended. Franzius and Juergens reported that CT is superior for the detection of pulmonary metastases and the mediastinal and hilar lymph node status [36]. If relevant for tumour staging, an additional CT of the thorax especially in soft tissue/bone sarcoma is recommended. Nowadays, the majority of ^{18}F-FDG PET examinations are performed as ^{18}F-FDG PET/CT; hence, an additional separate CT of the thorax will not be necessary during follow-up in future. However, in selected cases, a diagnostic CT of the thorax with breath-holding in inspiration has to be added to the low-dose attenuation correction CT during the same imaging session. In addition, a hybrid ^{18}F-FDG PET/CT could identify anatomical structures of ^{18}F-FDG PET-positive lesions and therefore reduce the number of false-positive findings. However, MRI offers a superior soft tissue contrast compared to CT [14]. MRI led to five false-negative scans mainly in bone/bone marrow lesions. ^{18}F-FDG PET demonstrated all of these active bone marrow lesions. Combined and registered ^{18}F-FDG PET/MRI helped to adjust false-negative scans on ^{18}F-FDG PET especially in ^{18}F-FDG PET inaccessible regions. In the follow-up, the specificity of an imaging modality is particularly important in order to avoid unnecessary biopsies or surgery. MRI alone resulted in an overly high number of false-positive scans in our patients. In the majority of persistent morphological tissue changes the scan was true-negative on ^{18}F-FDG PET. ^{18}F-FDG PET resulted in a specificity of 81 %, which was significantly higher than the specificity of 71 % of combined imaging (p=0.008), 72 % of registered imaging (p=0.019) and 30 % of MRI alone (p<0.001). In most cases, the false-positive ^{18}F-FDG PET scan occurred in patients with uptake in inflammatory tissue, physiological structures and post-therapeutic changes. In those cases, however, clinical signs and laboratory findings typical for inflammatory disease are often helpful for performing a short-term follow-up examination instead of an immediate biopsy. In a patient with Ewing sarcoma, both imaging modalities and combined imaging were false-positive. Only image registration could prove disease remission: The morphological changes could be identified as post-treatment residual oedematous tissue and the increased ^{18}F-FDG PET uptake as reactivated bone marrow after chemotherapy (Fig. 5).

Limitations

In our retrospective study the heterogeneous patient cohort with a huge variety of tumour entities made it difficult to compare single tumour entities within our study group and to other published studies. Most studies focus on a single malignancy. Lesion-based analyses are of limited use for treatment decisions: clinical classification systems such as the Ann Arbor system for lymphoma [37] and the TNM classification for solid tumours proposed by the American Joint Committee on Cancer [38] are widely used and determine therapeutic decisions. Those classification systems do not require detection of every single lesion, even in cases of a solitary lesion. However, lesion-based analyses are important to evaluate the diagnostic accuracy of imaging modalities. Considering the clinical impact of our study, we included an examination-related evaluation. Histopathological findings were not available for every lesion; however, at primary diagnosis every malignancy was proven histopathologically. In patients suffering from diffuse metastatic disease, a histological verification of every single lesion is impossible [39]. Within our setting, we assumed a lesion to be negative if it did not show any changes in behaviour, size or ^{18}F-FDG uptake without tumour-specific therapy over a period of 6 months. Non-detectable lesions on ^{18}F-FDG PET or MRI cannot be distinguished from nonexistent lesions in the case of a newly detected tumour lesion during follow-up. Therefore, the sensitivity will be overestimated, as seen in our study, with a value of 100 % in combined and registered ^{18}F-FDG PET/MRI analysis at primary diagnosis. The specificity of an imaging modality includes information on the detection of true-negative findings. At the time of primary diagnosis the number of true-negative findings was very low because most patients were suffering from vital tumour disease. In order to avoid distorting the specificity, we did not calculate it for the primary diagnosis in this context. Due to the rating of the modality with the higher diagnostic confidence score, there might be an unfair disadvantage for combined and registered ^{18}F-FDG PET/MRI compared to the modalities alone. Several patients were examined in various follow-up examinations. The fact that some lesions were evaluated more than once could have led to a distortion of the results. In our study setting, all examinations were carried out on separate imaging devices. In the literature, similar image comparison was complicated by factors like breathing artefacts, variable filling of the bladder or slightly different body position [40]. Those factors could have influenced our image analysis and could probably be overcome with simultaneous image acquisition in a combined PET/MRI scanner.

Conclusion

For detection of single tumour lesions, registered ^{18}F-FDG PET/MRI proved to be the methodology of choice for adequate tumour staging in our patients. The future will show whether combined ^{18}F-FDG PET/MR scanners with simultaneous image acquisition have the potential to further reduce movement artefacts, misinterpretations due to physiological changes and the number of sedations. In the

examination-based evaluation, which is most important for patient management, MRI alone performed better than ^{18}F-FDG PET, combined and registered imaging during primary diagnosis. Furthermore, MRI is needed for exact intervention planning. In the follow-up, however, examination-based evaluation demonstrated a superiority of ^{18}F-FDG PET alone, especially when taking into account the few limitations of ^{18}F-FDG PET in case of suspected lesions located in the region of the urinary bladder and in case of movement artefacts.

Due to our findings, MRI is recommended as the method of choice during primary diagnosis and should be complemented by ^{18}F-FDG PET in case of multifocal disease. On the other hand, during follow-up, ^{18}F-FDG PET is most important. Additional low-dose or ultra-low-dose CT, which is used for attenuation correction in modern PET/CT scanners, has to prove whether further improvements of ^{18}F-FDG PET results can be achieved during follow-up. As therapy response monitoring becomes more and more important in paediatric oncology, there might be an increasing part for combined ^{18}F-FDG PET/MRI during primary diagnosis, as the initial tumoural ^{18}F-FDG uptake is indispensable in addition to the morphological information from MRI.

Conflicts of interest None.

References

1. Smith MA, Seibel NL, Altekruse SF, Ries LA, Melbert DL, O'Leary M, et al. Outcomes for children and adolescents with cancer: challenges for the twenty-first century. J Clin Oncol 2010;28:2625–34.
2. Schiepers C, Dahlbom M. Molecular imaging in oncology: the acceptance of PET/CT and the emergence of MR/PET imaging. Eur Radiol 2011;21:548–54.
3. Beyer T, Townsend DW, Brun T, Kinahan PE, Charron M, Roddy R, et al. A combined PET/CT scanner for clinical oncology. J Nucl Med 2000;41:1369–79.
4. Fletcher JW, Djulbegovic B, Soares HP, Siegel BA, Lowe VJ, Lyman GH, et al. Recommendations on the use of 18F-FDG PET in oncology. J Nucl Med 2008;49:480–508.
5. Zaidi H, Del Guerra A. An outlook on future design of hybrid PET/MRI systems. Med Phys 2011;38:5667–89.
6. Kleis M, Daldrup-Link H, Matthay K, Goldsby R, Lu Y, Schuster T, et al. Diagnostic value of PET/CT for the staging and restaging of pediatric tumors. Eur J Nucl Med Mol Imaging 2009;36:23–36.
7. London K, Cross S, Onikul E, Dalla-Pozza L, Howman-Giles R. 18F-FDG PET/CT in paediatric lymphoma: comparison with conventional imaging. Eur J Nucl Med Mol Imaging 2011;38:274–84.
8. Mawlawi O, Townsend DW. Multimodality imaging: an update on PET/CT technology. Eur J Nucl Med Mol Imaging 2009;36 Suppl 1:S15–29.
9. Brix G, Lechel U, Glatting G, Ziegler SI, Münzing W, Müller SP, et al. Radiation exposure of patients undergoing whole-body dual-modality 18F-FDG PET/CT examinations. J Nucl Med 2005;46:608–13.
10. Kleinerman RA. Cancer risks following diagnostic and therapeutic radiation exposure in children. Pediatr Radiol 2006;36 Suppl 2:121–5.
11. Pichler BJ, Kolb A, Nägele T, Schlemmer HP. PET/MRI: paving the way for the next generation of clinical multimodality imaging applications. J Nucl Med 2010;51:333–6.
12. Darge K, Jaramillo D, Siegel MJ. Whole-body MRI in children: current status and future applications. Eur J Radiol 2008;68:289–98.
13. Antoch G, Vogt FM, Freudenberg LS, Nazaradeh F, Goehde SC, Barkhausen J, et al. Whole-body dual-modality PET/CT and whole-body MRI for tumor staging in oncology. JAMA 2003;290:3199–206.
14. von Schulthess GK, Schlemmer HP. A look ahead: PET/MR versus PET/CT. Eur J Nucl Med Mol Imaging 2009;36 Suppl 1: S3–9.
15. Judenhofer MS, Wehrl HF, Newport DF, Catana C, Siegel SB, Becker M, et al. Simultaneous PET-MRI: a new approach for functional and morphological imaging. Nat Med 2008;14:459–65.
16. Eiber M, Martinez-Möller A, Souvatzoglou M, Holzapfel K, Pickhard A, Löffelbein D, et al. Value of a Dixon-based MR/PET attenuation correction sequence for the localization and evaluation of PET-positive lesions. Eur J Nucl Med Mol Imaging 2011;38:1691–701.
17. Boss A, Bisdas S, Kolb A, Hofmann M, Ernemann U, Claussen CD, et al. Hybrid PET/MRI of intracranial masses: initial experiences and comparison to PET/CT. J Nucl Med 2010;51:1198–205.
18. Stauss J, Franzius C, Pfluger T, Juergens KU, Biassoni L, Begent J, et al. Guidelines for 18F-FDG PET and PET-CT imaging in paediatric oncology. Eur J Nucl Med Mol Imaging 2008;35:1581–8.
19. Lucignani G, Paganelli G, Bombardieri E. The use of standardized uptake values for assessing FDG uptake with PET in oncology: a clinical perspective. Nucl Med Commun 2004;25:651–6.
20. Wegner EA, Barrington SF, Kingston JE, Robinson RO, Ferner RE, Taj M, et al. The impact of PET scanning on management of paediatric oncology patients. Eur J Nucl Med Mol Imaging 2005;32:23–30.
21. Goethals I, Hoste P, De Vriendt C, Smeets P, Verlooy J, Ham H. Time-dependent changes in 18F-FDG activity in the thymus and bone marrow following combination chemotherapy in paediatric patients with lymphoma. Eur J Nucl Med Mol Imaging 2010;37:462–7.
22. Przkora R, Perez-Canto A, Ertel W, Heyde CE. Ganglioneuroma: primary tumor or maturation of a suspected neuroblastoma? Eur Spine J 2006;15:363–5.
23. Dimitrakopoulou-Strauss A, Strauss LG, Heichel T, Wu H, Burger C, Bernd L, et al. The role of quantitative 18F-FDG PET studies for the differentiation of malignant and benign bone lesions. J Nucl Med 2002;43:510–8.
24. Aoki J, Watanabe H, Shinozaki T, Takagishi K, Ishijima H, Oya N, et al. FDG PET of primary benign and malignant bone tumors: standardized uptake value in 52 lesions. Radiology 2001;219:774–7.
25. Kumar R, Halanaik D, Malhotra A. Clinical applications of positron emission tomography-computed tomography in oncology. Indian J Cancer 2010;47:100–19.
26. Shreve PD, Anzai Y, Wahl RL. Pitfalls in oncologic diagnosis with FDG PET imaging: physiologic and benign variants. Radiographics 1999;19:61–77.
27. Weisdorf DJ, Craddock PR, Jacob HS. Glycogenolysis versus glucose transport in human granulocytes: differential activation in phagocytosis and chemotaxis. Blood 1982;60:888–93.
28. Montravers F, McNamara D, Landman-Parker J, Grahek D, Kerrou K, Younsi N, et al. [(18)F]FDG in childhood lymphoma: clinical

utility and impact on management. Eur J Nucl Med Mol Imaging 2002;29:1155–65.
29. London K, Stege C, Cross S, Onikul E, Graf N, Kaspers G, et al. 18F-FDG PET/CT compared to conventional imaging modalities in pediatric primary bone tumors. Pediatr Radiol 2012;42:418–30.
30. Ratib O, Beyer T. Whole-body hybrid PET/MRI: ready for clinical use? Eur J Nucl Med Mol Imaging 2011;38:992–5.
31. Hoffer FA. Magnetic resonance imaging of abdominal masses in the pediatric patient. Semin Ultrasound CT MR 2005;26:212–23.
32. Foster K, Chapman S, Johnson K. MRI of the marrow in the paediatric skeleton. Clin Radiol 2004;59:651–73.
33. Baba S, Abe K, Isoda T, Maruoka Y, Sasaki M, Honda H. Impact of FDG-PET/CT in the management of lymphoma. Ann Nucl Med 2011;25:701–16.
34. Daldrup-Link HE, Franzius C, Link TM, Laukamp D, Sciuk J, Jürgens H, et al. Whole-body MR imaging for detection of bone metastases in children and young adults: comparison with skeletal scintigraphy and FDG PET. AJR Am J Roentgenol 2001;177:229–36.
35. Mody RJ, Bui C, Hutchinson RJ, Yanik GA, Castle VP, Frey KA, et al. FDG PET imaging of childhood sarcomas. Pediatr Blood Cancer 2010;54:222–7.
36. Franzius C, Juergens KU. PET/CT in paediatric oncology: indications and pitfalls. Pediatr Radiol 2009;39 Suppl 3:446–9.
37. Carbone PP, Kaplan HS, Musshoff K, Smithers DW, Tubiana M. Report of the Committee on Hodgkin's Disease Staging Classification. Cancer Res 1971;31:1860–1.
38. Edge SB, Byrd DR, Compton CC, Fritz AG, Greene FL, Trotti A. AJCC cancer staging manual. 7th ed. New York: Springer; 2010. p. 1–646.
39. Depas G, De Barsy C, Jerusalem G, Hoyoux C, Dresse MF, Fassotte MF, et al. 18F-FDG PET in children with lymphomas. Eur J Nucl Med Mol Imaging 2005;32:31–8.
40. Loeffelbein DJ, Souvatzoglou M, Wankerl V, Martinez-Möller A, Dinges J, Schwaiger M, et al. PET-MRI fusion in head-and-neck oncology: current status and implications for hybrid PET/MRI. J Oral Maxillofac Surg 2012;70:473–83.

Eur J Nucl Med Mol Imaging (2011) 38:1648–1658
DOI 10.1007/s00259-011-1843-8

ORIGINAL ARTICLE

^{123}I-MIBG scintigraphy/SPECT versus ^{18}F-FDG PET in paediatric neuroblastoma

Henriette Ingrid Melzer · Eva Coppenrath · Irene Schmid · Michael H. Albert · Dietrich von Schweinitz · Coral Tudball · Peter Bartenstein · Thomas Pfluger

Received: 5 April 2011 / Accepted: 2 May 2011 / Published online: 27 May 2011

Abstract
Purpose To analyse different uptake patterns in ^{123}I-MIBG scintigraphy/SPECT imaging and ^{18}F-FDG PET in paediatric neuroblastoma patients.
Methods We compared 23 ^{123}I-MIBG scintigraphy scans and 23 ^{18}F-FDG PET scans (mean interval 10 days) in 19 patients with a suspected neuroblastic tumour (16 neuroblastoma, 1 ganglioneuroblastoma, 1 ganglioneuroma and 1 opsomyoclonus syndrome). SPECT images of the abdomen or other tumour-affected regions were available in all patients. Indications for ^{18}F-FDG PET were a ^{123}I-MIBG-negative tumour, a discrepancy in ^{123}I-MIBG uptake compared to the morphological imaging or imaging results inconsistent with clinical findings. A lesion was found by ^{123}I-MIBG scintigraphy and/or ^{18}F-FDG PET and/or morphological imaging.
Results A total of 58 suspicious lesions (mean lesion diameter 3.8 cm) were evaluated and 18 were confirmed by histology and 40 by clinical follow-up. The sensitivities of ^{123}I-MIBG scintigraphy and ^{18}F-FDG PET were 50% and 78% and the specificities were 75% and 92%, respectively. False-positive results (three ^{123}I-MIBG scintigraphy, one ^{18}F-FDG PET) were due to physiological uptake or posttherapy changes. False-negative results (23 ^{123}I-MIBG scintigraphy, 10 ^{18}F-FDG PET) were due to low uptake and small lesion size. Combined ^{123}I-MIBG scintigraphy/^{18}F-FDG PET imaging showed the highest sensitivity of 85%. In 34 lesions the ^{123}I-MIBG scintigraphy and morphological imaging findings were discrepant. ^{18}F-FDG PET correctly identified 32 of the discrepant findings. Two bone/bone marrow metastases were missed by ^{18}F-FDG PET.
Conclusion ^{123}I-MIBG scintigraphy and ^{18}F-FDG PET showed noticeable differences in their uptake patterns. ^{18}F-FDG PET was more sensitive and specific for the detection of neuroblastoma lesions. Our findings suggest that a ^{18}F-FDG PET scan may be useful in the event of discrepant or inconclusive findings on ^{123}I-MIBG scintigraphy/SPECT and morphological imaging.

Keywords ^{123}I-MIBG scintigraphy · ^{18}F-FDG PET · Neuroblastoma · Paediatrics

H. I. Melzer (✉) · P. Bartenstein · T. Pfluger
Department of Nuclear Medicine,
Ludwig Maximilian University of Munich,
Ziemssenstraße 1,
80336 Munich, Germany
e-mail: henriette.melzer@campus.lmu.de

E. Coppenrath
Department of Radiology,
Ludwig Maximilian University of Munich,
Munich, Germany

I. Schmid · M. H. Albert
Department of Paediatric Haematology/Oncology,
Ludwig Maximilian University of Munich,
Munich, Germany

D. von Schweinitz
Department of Paediatric Surgery,
Ludwig Maximilian University of Munich,
Munich, Germany

C. Tudball
Department of Nuclear Medicine, Royal Children's Hospital,
Melbourne, VIC, Australia

Introduction

Neuroblastoma accounts for about 8% of paediatric malignancies and is responsible for approximately 15% of cancer deaths in children [1, 2]. At diagnosis, roughly 50%

of the patients have distant metastases [3]. The 5-year event-free survival rate strongly depends upon age, molecular markers and the stage of disease [4]. It ranges from 99% in stage I to about 45% in stage IV disease [5, 6]. Therefore staging is crucial for appropriate treatment [7].

Due to its neuroendocrine origin, the malignancy takes up catecholamines and related substances. The catecholamine analogue ^{123}I-meta-iodobenzylguanidine (^{123}I-MIBG) is widely used to image tumours of the sympathetic nervous system and ^{123}I-MIBG scintigraphy is well established for staging and evaluation of therapeutic response [8, 9]. However, the assessment of MIBG scans presents some difficulties: false-negative MIBG scans were reported as early as 1990 [10], and false-negative ^{123}I-MIBG scintigraphy is still a problem, and may lead to incorrect down-staging [7]. In about 8% of neuroblastoma patients MIBG scintigraphy gives a false-negative result at diagnosis, even though there is clear evidence of disease [11]. In particular, MIBG scintigraphy gives a false result concerning bone marrow involvement [12]. The coexistence of hot and cold ^{123}I-MIBG lesions still remains unclear.

Positron emission tomography with ^{18}F-fluorodeoxyglucose (^{18}F-FDG PET) depicts the metabolic state of cancer cells and provides information on the malignant potential of the disease [13]. ^{18}F-FDG PET findings correlate well with the disease status [14]. Nevertheless, ^{18}F-FDG PET has rarely been used in the context of neuroblastic tumours. Neuroblastomas concentrate ^{18}F-FDG before cytoreductive therapy, whereas intra- and posttherapeutic uptake is variable [13]. Sharp et al. found ^{18}F-FDG PET to be useful in low stage neuroblastoma in patients with tumours that weakly accumulate ^{123}I-MIBG and at major decision points during therapy [15].

The aim of this retrospective study was to investigate the usefulness of ^{18}F-FDG PET in a preselected population of patients with neuroblastoma and with inconclusive or inconsistent results on ^{123}I-MIBG scintigraphy/SPECT imaging and morphological imaging.

Materials and methods

Search algorithm

From July 2004 to July 2010, 245 ^{123}I-MIBG scintigraphy scans were performed in 108 patients with proven or suspected neuroblastic tumours, and 42 ^{18}F-FDG PET scans were performed in the same group during the same time period. ^{18}F-FDG PET was performed if there was a ^{123}I-MIBG-negative tumour, a discrepancy in the ^{123}I-MIBG uptake compared to morphological imaging, or results inconsistent with the clinical findings. The inclusion criterion for the study was a maximum period of 30 days (mean 10 days, range 0–30 days) between ^{123}I-MIBG scintigraphy, ^{18}F-FDG PET and morphological imaging. If there was no coincident morphological study available, the patient was excluded. Patients with a proven diagnosis other than neuroblastoma, ganglioneuroblastoma, or ganglioneuroma were excluded. Examinations were performed either before or at least 6 weeks after chemotherapy. Patients were excluded if there had been any tumour-specific therapy between ^{123}I-MIBG scintigraphy and ^{18}F-FDG PET. Histopathology and/or clinical follow-up data for each lesion had to be available. Thus, 23 instances in 19 patients met the inclusion criteria.

Patients

Simultaneously 23 ^{123}I-MIBG scintigraphy scans and 23 ^{18}F-FDG PET scans were performed in 19 paediatric patients (ten male and nine female; mean age 5 years 11 months; age range 8 months to 19 years 1 month) and analysed retrospectively. Six combined ^{123}I-MIBG scintigraphy scans and ^{18}F-FDG PET scans were performed for initial staging and 17 during follow-up. Of the 19 patients, 16 had histologically proven neuroblastoma, 1 ganglioneuroblastoma, 1 ganglioneuroma and 1 opsomyoclonus syndrome. According to the International Neuroblastoma Staging System [16], patients were classified as stage I (3 patients), stage IIA (1), stage III (3) and stage IV (11). The patient with opsomyoclonus syndrome was not categorized. Concerning bone and bone marrow involvement, ^{123}I-MIBG scintigraphy scans were ranked according to the SIOPEN classification system [17]. The skeleton was divided into 12 anatomical sections and a score from 0 to 6 was assigned to each section: score 0 (17 scans), 1 (2 scans), 2 (1 scan), 4 (1 scan), 5 (1 scan) and 19 (1 scan). In molecular testing, three neuroblastomas showed MYCN oncogene amplification and 1p deletion, 14 tumours were MYCN-negative and in one patient the MYCN amplification status was unknown.

Acquisition protocol

^{123}I-MIBG scans were performed under thyroid blockade with perchlorate over 3 days, starting 30–60 min before administration of ^{123}I-MIBG at a dose of 10 mg/kg per day. The administered dose of ^{123}I-MIBG was adapted to body weight according to the dosage card of the EANM [18]. A dual-head gamma camera (Prism 2000 XP; Philips Medical Systems, Best, The Netherlands) was used with a medium-energy collimator. Imaging was performed 24 h after slow intravenous injection of ^{123}I-labelled MIBG (spot images of the whole body, matrix 256×256 pixels, dorsal/ventral view, maximum acquisition time per image 10 min; above

120 cm body size whole-body scan with a table feed of 6 cm/min). In all patients, SPECT images of the abdomen or other tumour-affected regions were available (3° steps, 2×180°; 15 s per step; matrix 128×128 pixels).

^{18}F-FDG PET scans were acquired with a Philips Allegro PET scanner. All patients fasted for at least 4 h and blood glucose levels were determined to monitor for deviation from normal levels prior to ^{18}F-FDG PET imaging. Furosemide and butylscopolamine were administrated to minimize physiological activity in the bowel and bladder. ^{18}F-FDG was injected intravenously 1 h before scanning at a dose according to body weight and the guidelines of the EANM [19], and the patient was instructed to rest until the beginning of the examination. PET was performed using three to ten bed positions (depending on the size of the patient) with a 2-min acquisition time per bed position. Images were attenuation-corrected and were acquired in 3-D mode using a row action maximum likelihood algorithm (3D RAMLA). The examination field-of-view was the whole body. To avoid motion artefacts, sedation was necessary in 6 of the 23 examinations.

Image analysis

Lesion-based image analysis was performed. A lesion was included in the analysis if it was considered positive for neuroblastoma involvement on ^{123}I-MIBG scintigraphy, ^{18}F-FDG PET or morphological imaging. Individual data analyses of both nuclear medicine modalities were performed by three independent observers, two for the ^{123}I-MIBG imaging and one for the ^{18}F-FDG PET. Images were analysed with knowledge of the clinical data, but without knowledge of the findings of the other imaging modality. To determine whether regression or disappearance of lesions was evident on follow-up examinations, observers needed to know the findings from the previous examination of the same modality. Combined assessment of both modalities was performed by the same three observers after the separate analyses.

^{123}I-MIBG scans and ^{18}F-FDG PET images were reviewed on a HERMES workstation (Nuclear Diagnostics, Haegersten, Sweden). After combined ^{123}I-MIBG scintigraphy/^{18}F-FDG PET evaluation, the same three observers compared the findings with morphological imaging (18 MRI scans, 5 CT scans).

A total of 58 lesions were evaluated. Two patients had several examination pairs; hence 12 lesions were reanalysed in at least one (up to three) follow-up examinations. A lesion was classified a "primary tumour" if it occurred in the adrenal gland, the sympathetic trunk or local recurrence of the original tumour was found. All other lesions were considered "metastases". In both modalities, each lesion was judged either positive or negative with regard to tumour involvement. On the ^{123}I-MIBG scintigraphy scans, a lesion was judged positive if nonphysiological focal uptake was seen. For semiquantitative analysis, the maximum count rate of each lesion was noted, and divided by the maximum count rate of the patient's right liver lobe. This count rate ratio (CRR) was used to establish a diagnostic confidence score. On the ^{18}F-FDG PET scans, a lesion was judged positive if it showed nonphysiological glucose metabolism. For the diagnostic confidence score, the maximum standardized uptake value (SUV_{max}) of each lesion was determined.

To reach a decision on lesions with discrepant results in the combined image analysis, a diagnostic confidence score with three levels was established for each modality:

1. ^{123}I-MIBG scintigraphy (CRR <1), ^{18}F-FDG PET (SUV_{max} <1)
2. ^{123}I-MIBG scintigraphy (CRR 1–1.5), ^{18}F-FDG PET (SUV_{max} 1–2)
3. ^{123}I-MIBG scintigraphy (CRR >1.5), ^{18}F-FDG PET (SUV_{max} >2)

This diagnostic confidence score was assigned to each suspicious lesion on ^{123}I-MIBG scintigraphy and ^{18}F-FDG PET scans separately. If there was a discrepancy between the two modalities, the finding of the modality with the higher diagnostic confidence level was used. If both modalities were discrepant and revealed the same score, the lesion was judged positive.

Standard of reference

The standard of reference was the histopathological findings of the lesion (18 lesions) or by follow-up evaluation (40 lesions). In particular, for patients with stage IV neuroblastoma, histopathological verification of all metastases is impossible. Therefore, follow-up examinations after a minimum period of 6 months were used for verification of the lesions: MRI (20 lesions) or CT (3 lesions) and/or ^{123}I-MIBG scintigraphy (17 lesions) and/or ^{18}F-FDG PET (12 lesions). A lesion was classified as either "false-positive" or "true-negative" if it disappeared without tumour therapy during the observation period. A lesion was classified as either "true-positive" or "false-negative" if it persisted or progressed during follow-up, or showed objective regression with specific therapy.

Results

A total of 58 lesions were evaluated, of which 46 (79%) proved to be vital tumour tissue. The anatomical lesion sites are shown in Table 1, and the morphological diameters

Table 1 Anatomical tumour site (n=58)

Anatomical site	Number of lesions	Primary tumour	Metastasis
Adrenal gland	15	15	–
Paravertebral region	6	6	–
Bone			
Scapula	2	–	2
Vertebral column	11	–	11
Pelvis	6	–	6
Femur/tibia	13	–	13
Lymph nodes			
Mediastinum	2	–	2
Retrocrural region	1	–	1
Presacral region	1	–	1
Other			
Central abdomen	1	–	1
Total	58	21	37

(mean lesion diameter 3.8 cm) and the lesion distribution according to the stage of disease are presented in Table 2. The lesion-based results are summarized in Table 3.

^{123}I-MIBG scintigraphy

^{123}I-MIBG scintigraphy showed false-positive findings in three patients due to physiological activity in a normal adrenal gland (two lesions; Fig. 1) and physiological bowel uptake (one lesion). They were found in patients with stage III disease (lesion diameter in the central abdomen >5 cm) and stage IV disease (lesion diameter in the adrenal gland <1 cm) and in the patient with opsomyoclonus syndrome (lesion diameter in the adrenal gland 1–2 cm).

False-negative results (23 lesions; mean lesion diameter 1.7 cm) occurred in bone/bone marrow metastases in the vertebral column (five lesions), pelvis (four lesions), femur (seven lesions), paravertebral region (three lesions), and adrenal region (four lesions; Fig. 2). The 23 false-negative findings are shown in relation to disease stage in Table 4.

Table 2 Lesion distribution according to stage, lesion diameter on MRI/CT, and false-negative findings

Stage	Diameter (cm)	Number of lesions	False-negative	
			^{123}I-MIBG scintigraphy	^{18}F-FDG PET
I (n=3)	1–2	1		
	2–5	1	2	0
	>5	1		
IIA (n=1)	2–5	1	0	1
III (n=4)	2–5	1	1	1
	>5	3		
IV (n=49)	<1	14		
	1–2	13	20	8
	2–5	15		
	>5	7		
Opsomyoclonus syndrome (n=1)	1–2	1	0	0

^{18}F-FDG PET

On ^{18}F-FDG PET, there was one false-positive finding in a patient with stage IV disease. This was seen in the adrenal region and was due to posttherapy uptake (lesion diameter <1 cm). With regard to false-negative findings (ten lesions; mean lesion diameter 1.6 cm), the following neuroblastoma lesions were missed: adrenal gland tumour (two lesions), bone/bone marrow metastases in the tibia/femur (three lesions), vertebral column (one lesion), retrocrural region (one lesion), presacral region (one lesion), paravertebral region (one lesion), and thymus (one lesion). These lesions could not be differentiated from physiological uptake and occurred in one patient with stage IIA disease (thymus, lesion diameter 2–5 cm), in one patient with stage III disease (presacral region, 2–5 cm) and in patients with stage IV disease (two lesions, adrenal gland, 2–5 cm; two lesions, tibia/femur, <1 cm; one lesion, tibia/femur, 1–2 cm; one lesion, vertebral column, 1–2 cm; one lesion, retrocrural region, 1–2 cm; one lesion, paravertebral region, 2–5 cm).

MRI/CT

All 58 lesions were correlated morphologically with either MRI (52 lesions) or CT (6 lesions) scans. The nine following false-positive findings were obtained in patients with stage IV disease: region of the primary tumour in the adrenal gland (two lesions, lesion diameter <1 cm and 2–5 cm) due to posttherapy changes; bone/bone marrow involvement in the femur and pelvis (three lesions, lesion diameter <1 cm; one lesion, 1–2 cm; one lesion, 2–5 cm) and the vertebral column (two lesions, lesion diameter <1 cm and 2–5 cm) due to oedematous nonviable residual tumour. Three false-negative findings occurred in patients with stage IV disease. These were located in the femur (one) and the vertebral column (two) because of small tumour size (Fig. 3).

Comparison of ^{123}I-MIBG scintigraphy and ^{18}F-FDG PET

In 33 lesions, discrepancies between ^{123}I-MIBG scintigraphy and ^{18}F-FDG PET were found. In 29 of these 33

Table 3 Imaging findings in primary diagnosis and follow-up (n=58)

Finding	^{123}I-MIBG scintigraphy			^{18}F-FDG PET			^{123}I-MIBG scintigraphy and ^{18}F-FDG PET			CT or MRI		
	Primary diagnosis	Follow-up examination	Total	Primary diagnosis	Follow-up examination	Total	Primary diagnosis	Follow-up examination	Total	Primary diagnosis	Follow-up examination	Total
True-positive	11	12	23	20	16	36	19	20	39	18	25	43
True-negative	0	9	9	1	10	11	1	10	11	1	2	3
False-positive	1	2	3	0	1	1	0	1	1	0	9	9
False-negative	10	13	23	1	9	10	2	5	7	3	0	3
Sensitivity (%)	52	48	50	95	64	78	90	80	85	86	100	93
Specificity (%)	–	82	75	100	91	92	100	91	92	100	18	25

lesions, vital tumour lesions could only be detected by one modality (8 by ^{123}I-MIBG scintigraphy, 21 by ^{18}F-FDG PET; Fig. 4). Four of these 33 lesions were classified as true-negative by only one modality (one by ^{123}I-MIBG scintigraphy, three by ^{18}F-FDG PET).

Combining the two modalities, one false-positive and seven false-negative results remained. Physiological adrenal ^{123}I-MIBG uptake was misinterpreted as residual vital tumour tissue after surgery in one patient. Seven false-negative findings were either due to a misinterpretation of viable tumour lesions as postoperative changes in the adrenal gland region (two lesions, lesion diameter 2–5 cm and >5 cm) or due to small size and/or low metabolic activity in bone marrow metastases in the vertebral column (one lesion, lesion diameter <1 cm), in the femur (two lesions, lesion diameter <1 cm). Two

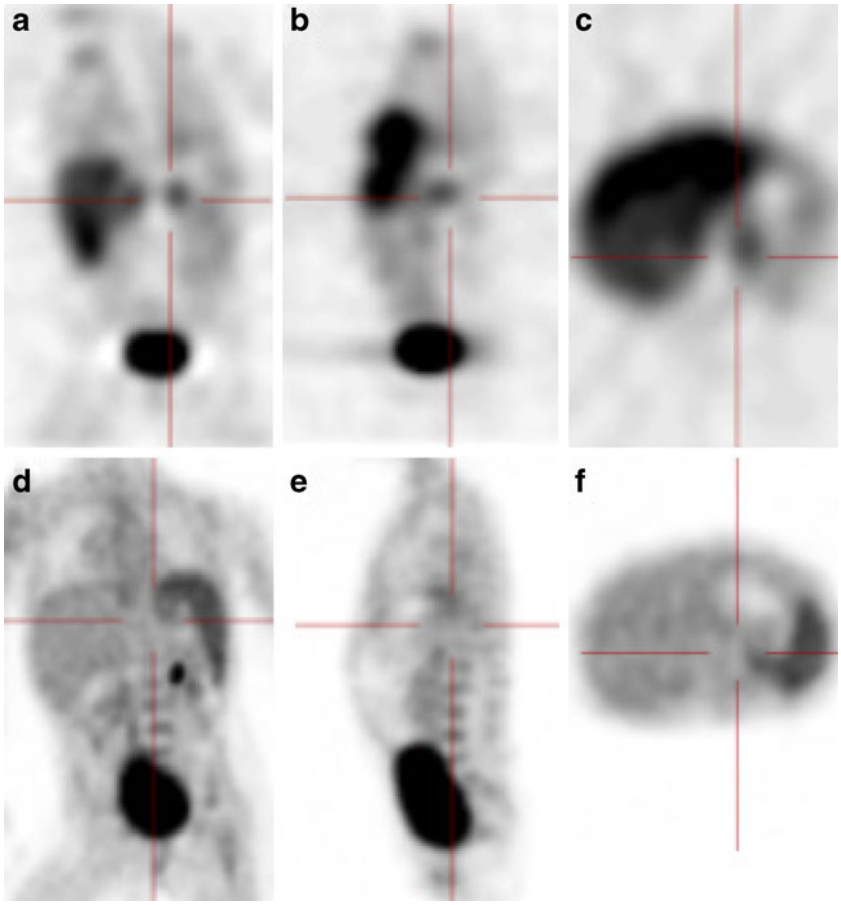

Fig. 1 A 1½-year old girl with neuroblastoma at the follow-up evaluation 3 months after the end of chemotherapy with a false-positive finding on ^{123}I-MIBG scintigraphy. ^{123}I-MIBG scintigraphy images show a suspect lesion in the region of the left adrenal gland (**a**–**c**). The corresponding ^{18}F-FDG PET images are true-negative with no increased uptake (**d**–**f**), indicating that the changes seen on ^{123}I-MIBG scintigraphy are physiological

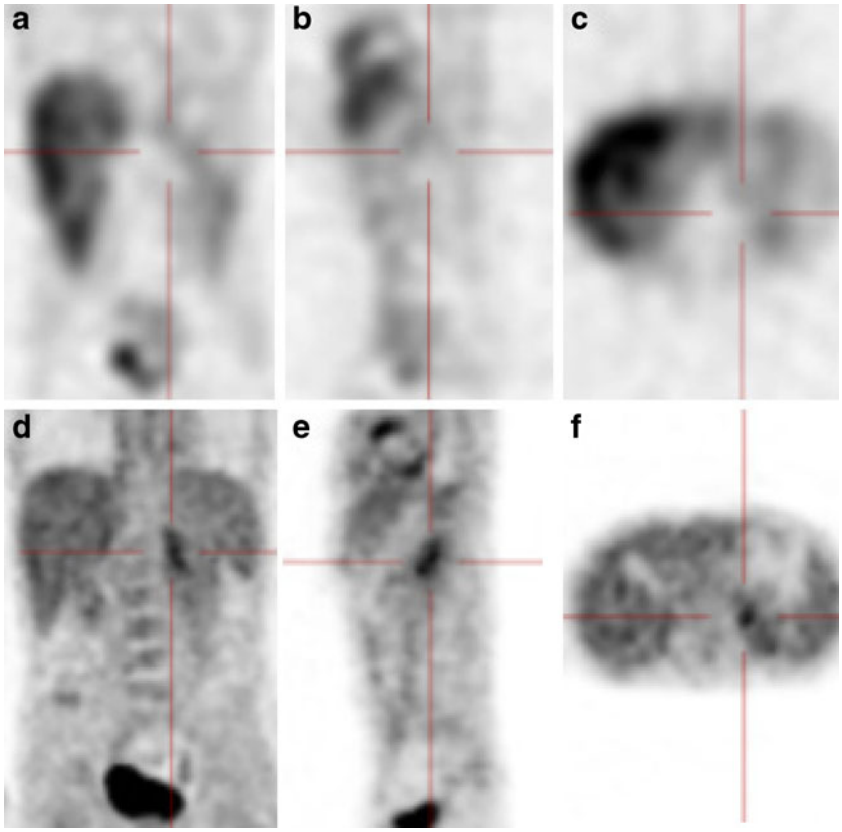

Fig. 2 A 7-year-old girl with recurrent neuroblastoma and false-negative finding on ^{123}I-MIBG scintigraphy. The ^{123}I-MIBG scintigraphy images do not show recurrent disease (**a–c**) but the ^{18}F-FDG PET images show a lesion in the left adrenal region (**d–f**). The lesion was histopathologically confirmed

metastases were misinterpreted as physiological uptake: a retrocrural lymph node metastasis (lesion diameter 1–2 cm) and a metastasis in the thymus (lesion diameter 2–5 cm).

Table 4 23 false-negative findings on ^{123}I-MIBG scintigraphy in relation to disease stage

Stage	Lesion		No. of lesions
	Anatomical site	Diameter (cm)	
I (n=2)	Adrenal gland	1–2	1
		>5	1
III (n=1)	Paravertebral region	>5	1
IV (n=20)	Vertebral column	<1	2
		1–2	2
		2–5	1
	Pelvis	1–2	1
		2–5	2
		>5	1
	Femur	<1	4
		1–2	3
	Paravertebral region	2–5	2
	Adrenal gland	1–2	1
		2–5	1

Comparison of ^{123}I-MIBG scintigraphy and morphological imaging

The comparison of ^{123}I-MIBG scintigraphy and morphological imaging modalities resulted in 34 discrepant findings (Table 5).

In the primary diagnosis, 12 discrepant results were found. In all 12 lesions, ^{18}F-FDG PET was the modality that provided the correct evaluation (Fig. 5). In the follow-up, ^{123}I-MIBG scintigraphy and morphology showed 22 discrepant findings. In 20 lesions ^{18}F-FDG PET was the modality that provided the correct evaluation of the lesion.

Two bone/bone marrow lesions in the proximal femur were incorrectly classified by both functional imaging modalities; there was no discrepancy between ^{123}I-MIBG scintigraphy and ^{18}F-FDG PET. These lesions were seen on the MRI images (lesion diameter <1 cm).

Discussion

The question as to whether the detection of neuroblastoma lesions that are weakly or not affine to ^{123}I-MIBG can be improved by simultaneous ^{18}F-FDG PET was investigated by this retrospective study. The utility of the simultaneous use of ^{18}F-FDG PET and ^{123}I-MIBG scintigraphy in

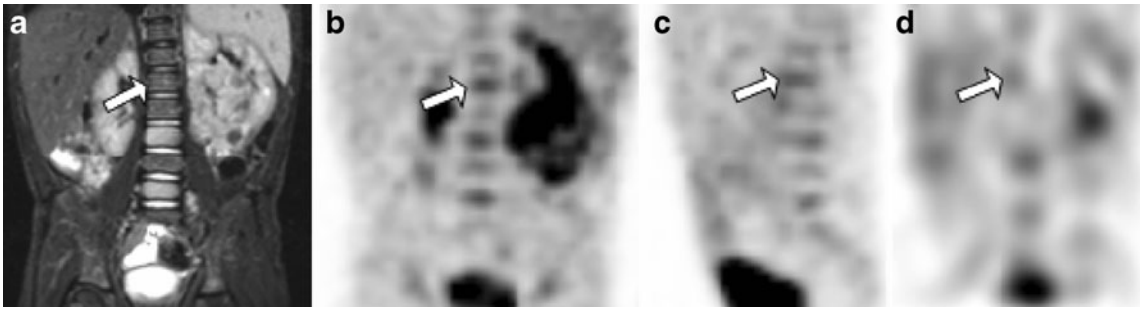

Fig. 3 A 4-year-old boy at primary diagnosis of a left-sided neuroblastoma with a false-negative finding on MRI. On the MRI image (T2-weighted STIR sequence) suspect bone/bone marrow lesions were found in vertebral bodies L3 and L5. L1 (*arrow*) does not show pathological changes (**a**), whereas on the ^{18}F-FDG PET images (**b**, **c**) and on the ^{123}I-MIBG scintigraphy image (**d**) a suspicious lesion is apparent in L1. In addition, the primary tumour mass is demonstrated by all three imaging modalities

children with neuroblastoma had already been assessed by Sharp et al. [15]. ^{18}F-FDG PET was found to be superior to ^{123}I-MIBG scintigraphy in children with stage I or II neuroblastoma, but inferior in patients with stage IV neuroblastoma, based on the International Neuroblastoma Staging System. ^{18}F-FDG PET provided additional information in the chest, abdomen and pelvis, and depicted neuroblastomas which did not accumulate or only weakly accumulated ^{123}I-MIBG. However, in patients with stage IV disease, ^{123}I-MIBG scintigraphy was superior to ^{18}F-FDG PET especially during initial chemotherapy [15]. In our study, false-positive and false-negative ^{18}F-FDG PET and ^{123}I-MIBG scintigraphy findings were distributed almost equally throughout all tumour stages. This may be due to the fact that patients were included in our study only if ^{123}I-MIBG scintigraphy and ^{18}F-FDG PET examinations had been performed before or at least 6 weeks after cytotoxic therapy. Shulkin et al. suggested that ^{18}F-FDG PET was inferior to ^{123}I-MIBG scintigraphy when used shortly after or during systematic therapy due to a lower

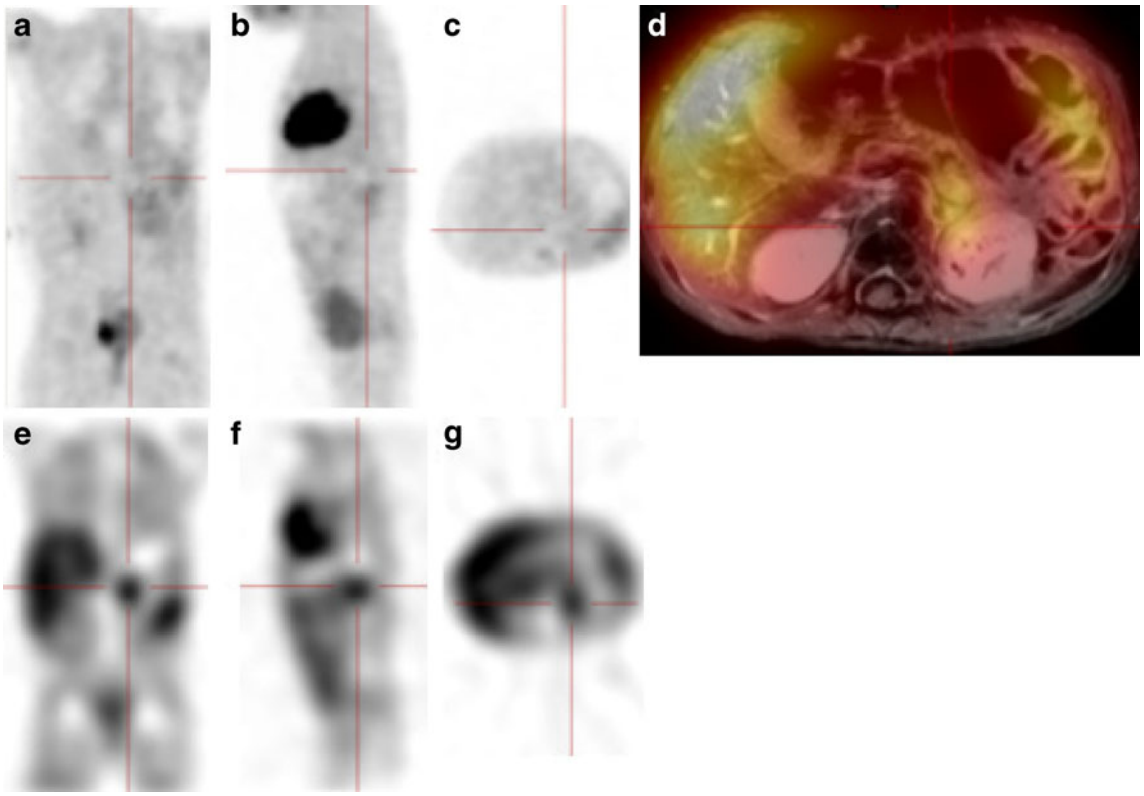

Fig. 4 A 2-year-old girl with a left-sided persistent neuroblastoma after surgery and chemotherapy and a false-negative finding on ^{18}F-FDG PET. In the ^{18}F-FDG PET images no suspicious lesion is seen in the region of the left adrenal gland (**a**–**c**). On the MRI image it is not possible to differentiate between posttherapy changes and viable tumour (**d**); however, on the ^{123}I-MIBG scintigraphy image pathological uptake is seen (**e**–**g**) indicating persistent tumour. The lesion was confirmed histopathologically

Table 5 Discrepant findings: ^{123}I-MIBG scintigraphy versus CT/MRI

Finding	^{123}I-MIBG scintigraphy	CT or MRI	^{18}F-FDG PET
True-positive	2	22	22
True-negative	8	2	10
False-positive	2	8	0
False-negative	22	2	2

tumour-to-nontumour uptake ratio and physiological ^{18}F-FDG accumulation [13].

Lesion-based analysis

^{123}I-MIBG scintigraphy showed an overall sensitivity of 50% and a specificity of 75% for the detection of neuroblastoma involvement. This is markedly lower than in a recently published multicentre trial and meta-analysis that confirmed a generally high sensitivity and specificity, mostly over 80% [20, 21]. These low values in our retrospective study are probably due to the fact that the patient population was preselected with a high number of negative or inconclusive findings on ^{123}I-MIBG scintigraphy scans. In this patient population, ^{18}F-FDG PET exhibited a notably higher sensitivity and specificity (78% and 92%, respectively) than ^{123}I-MIBG scintigraphy.

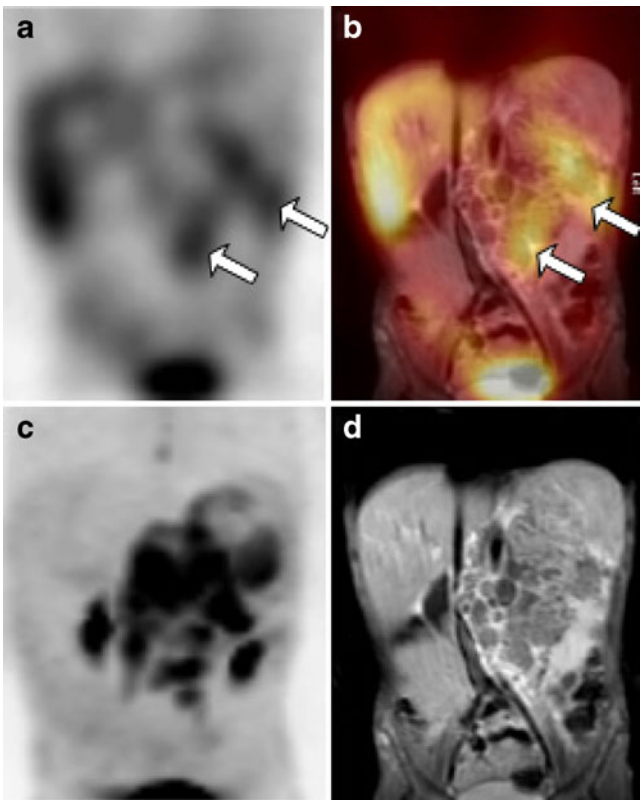

Fig. 5 A 3½-year-old boy at primary diagnosis of a stage IV neuroblastoma and discrepant findings on ^{123}I-MIBG scan and morphological imaging. ^{123}I-MIBG scintigraphy (**a** SPECT, **b** registered SPECT/MRI) only shows a slightly increased tracer uptake at the lower and lateral border of the tumour (*arrows*). However, ^{18}F-FDG PET (**c** maximum intensity projection) and MRI (**d**) images demonstrate extended bulky disease and ^{18}F-FDG hypermetabolism in the entire primary tumour

Most false-positive ^{123}I-MIBG scintigraphy findings are caused by nonspecific radioactive accumulation in the urinary tract and in gastrointestinal structures [22]. This was also the case in our study with false-positive uptake in the adrenal region and in the gastrointestinal tract. ^{18}F-FDG PET helped to correctly categorize these wrongly classified lesions.

False-negative ^{123}I-MIBG scintigraphy findings were mostly seen in bone and bone marrow, confirming the well-known fact that the sensitivity of ^{123}I-MIBG scans is limited in the detection of single bone and bone marrow metastases [22]. The SIOPEN classification system for bone or bone marrow involvement [17] enables the evaluation and standardized comparison of metastatic disease detected on ^{123}I-MIBG scans. Due to our patient selection with negative or inconclusive ^{123}I-MIBG scans, only low score values were expected in the SIOPEN classification. This does not reflect a particular weakness of the classification system. However, in our setting with many bone/bone marrow lesions that were false-negative on^{123}I-MIBG scintigraphy, the SIOPEN classification led to incorrect downstaging. Further false-negative lesions on ^{123}I-MIBG scintigraphy were located in the adrenal gland and in the sympathetic trunk. Possible reasons for these false-negative findings have been discussed in the literature, and include the absence of a mechanism by which ^{123}I-MIBG is transported into the tumour cells, small tumour size and the coexistence of various neoplastic clones with different uptake behaviour [11, 23].

^{18}F-FDG PET has been reported to be equal or superior to ^{123}I-MIBG scintigraphy for identifying neuroblastoma lesions in soft tissue and extracranial skeletal structures [24]. In our series, ^{18}F-FDG PET correctly identified almost all false-negative lesions as vital tumour tissue and proved its utility especially in lesions negative on ^{123}I-MIBG scintigraphy. Due to surrounding oedema, the two remaining false-negative lesions were shown on morphological imaging.

In false-negative findings, there was no significant difference between ^{123}I-MIBG scintigraphy and ^{18}F-FDG PET with regard to the morphological mean lesion diameter: 1.7 cm on ^{123}I-MIBG scintigraphy, 1.6 cm on ^{18}F-FDG PET. However, when looking at all 58 lesions, the mean morphological lesion diameter was 3.8 cm.

Primary diagnosis

At primary diagnosis, ^{18}F-FDG PET missed one lesion in the bone marrow of the vertebral column. It correctly

identified all lesions that were false-negative on ^{123}I-MIBG scintigraphy. As initial staging requires highly sensitive imaging modalities, ^{18}F-FDG PET proved to be a valuable additional staging examination in our study. Nevertheless, in a nonselected population of neuroblastoma patients, the sensitivity of ^{123}I-MIBG scintigraphy in primary diagnosis is around 90% [25]. Therefore, ^{123}I-MIBG scintigraphy remains a crucial initial staging modality. In primary diagnosis, morphological imaging is needed to evaluate operability and to detect bone marrow metastases with a high sensitivity [26]. In our study, however, three bone/bone marrow lesions were missed by MRI. All of them were correctly detected by ^{18}F-FDG PET; ^{123}I-MIBG scintigraphy showed only two of these bone/bone marrow lesions and missed one.

Follow-up

During follow-up, our lesion-based analysis showed a sensitivity of 48% vs. 64% and a specificity of 82% vs. 91% for ^{123}I-MIBG scintigraphy and ^{18}F-FDG PET. Difficulties assessing neuroblastoma lesions at follow-up have been discussed. Lesions positive on ^{123}I-MIBG scintigraphy at primary diagnosis that were negative on the ^{123}I-MIBG scan at relapse, although recurrence was proved, have been reported [27–29]. Possible reasons are primary negative lesions on ^{123}I-MIBG scintigraphy or tumour cells which survive chemotherapy and afterwards fail to accumulate ^{123}I-MIBG [30]. In disagreement with our results, Taggart et al. found ^{123}I-MIBG scintigraphy to be more sensitive than ^{18}F-FDG PET for individual anatomical lesion detection in relapsed neuroblastoma [31]. This difference may be due to our preselected patient population with many neuroblastoma lesions that were weakly affine to ^{123}I-MIBG. Consequently, in our series, ^{18}F-FDG PET was superior to ^{123}I-MIBG scintigraphy in the follow-up. Morphological imaging in the follow-up evaluation lacks specificity because vital residual disease is difficult to differentiate from necrotic tissue [32]. With a specificity of 18%, MRI/CT was not appropriate as a single imaging modality in the follow-up in our study.

^{123}I-MIBG scintigraphy and ^{18}F-FDG PET imaging combined

Combined imaging with ^{123}I-MIBG scintigraphy and ^{18}F-FDG PET was more sensitive than ^{18}F-FDG PET alone. However, on combining the two functional imaging modalities, eight incorrectly classified lesions remained. Postoperative changes and limited lesion size and/or low metabolic activity in the modality with the higher diagnostic confidence level were the main reasons for the false lesion classification. Of these eight lesions, six showed discrepant findings on ^{123}I-MIBG scintigraphy and ^{18}F-FDG PET. In discrepant ^{123}I-MIBG scintigraphy/^{18}F-FDG PET findings, comparison with morphological imaging should be performed in order to increase diagnostic safety in verifying subtle findings on the functional imaging [32]. In our study, only two falsely classified lesions in bone/bone marrow remained with concordant false-negative results on ^{123}I-MIBG scintigraphy and ^{18}F-FDG PET.

^{123}I-MIBG scintigraphy and MRI/CT imaging combined

In a clinical setting, morphological imaging is added to functional imaging to assess a patient's disease. Of 34 discrepant findings on ^{123}I-MIBG scintigraphy and morphological imaging, all but two were correctly identified by ^{18}F-FDG PET. They were false-negative bone/bone marrow lesions of small size in the femur that were shown on MRI due to tumoral oedema. A possible reason for negative ^{18}F-FDG PET findings is a nonmetabolic state during examination. In follow-up examinations both lesions showed a clear progression on ^{18}F-FDG PET.

On the other hand, in two lesions both ^{123}I-MIBG scintigraphy and morphological imaging produced equivalent false findings: false-negative in a bone/bone marrow lesion in the vertebral column and false-positive in the adrenal gland. The diagnostic confidence scores on ^{123}I-MIBG scintigraphy and morphological imaging for those two lesions were low, indicating equivocal findings. In both cases ^{18}F-FDG PET indicated the true finding.

On the basis of our results, ^{18}F-FDG PET is recommended as an additional imaging modality in the event of discrepancies or equivocal findings on ^{123}I-MIBG scintigraphy and morphological imaging.

Limitations

In our retrospective study, the number of included patients was small due to the maximum period of 30 days between imaging modalities and due to the pre-selection criterion of negative or inconclusive ^{123}I-MIBG scintigraphy. The majority of our patients suffered from stage IV disease. A multicentre approach investigating the possible use of ^{18}F-FDG PET in neuroblastomas negative on ^{123}I-MIBG scintigraphy could obtain a higher number of patients with a more homogeneous distribution of disease.

Moreover, the preselected patient group in our study does not represent the general population of patients with neuroblastoma. The sensitivity and specificity of ^{123}I-MIBG scintigraphy obtained in our study is not valid for the general population of patients with neuroblastoma. This makes it difficult to compare our results with studies already published in the literature.

The specificity of an imaging modality includes information on the detection of true-negative findings. The number of true-negative findings was very low because all but one of our patients suffered from vital tumour disease at the time of the primary diagnosis. In order to avoid distorting the specificity, we did not calculate it for the ^{123}I-MIBG scintigraphy in this context.

Conclusion

In this study with a preselected patient population, ^{123}I-MIBG scintigraphy and ^{18}F-FDG PET showed noticeable differences in their uptake patterns. ^{18}F-FDG PET was more sensitive and specific for the detection of neuroblastoma lesions that were weakly affine to ^{123}I-MIBG. Our results suggest that an ^{18}F-FDG PET scan can be recommended if there are discrepant or inconclusive findings on ^{123}I-MIBG scintigraphy/SPECT imaging and morphological imaging.

Conflicts of interest None.

References

1. Spix C, Aareleid T, Stiller C, Magnani C, Kaatsch P, Michaelis J. Survival of children with neuroblastoma. time trends and regional differences in Europe, 1978–1992. Eur J Cancer. 2001;37:722–9.
2. Taggart D, Dubois S, Matthay KK. Radiolabeled metaiodobenzylguanidine for imaging and therapy of neuroblastoma. Q J Nucl Med Mol Imaging. 2008;52:403–18.
3. DuBois SG, Kalika Y, Lukens JN, Brodeur GM, Seeger RC, Atkinson JB, et al. Metastatic sites in stage IV and IVS neuroblastoma correlate with age, tumor biology, and survival. J Pediatr Hematol Oncol. 1999;21:181–9.
4. Smith MA, Seibel NL, Altekruse SF, Ries LA, Melbert DL, O'Leary M, et al. Outcomes for children and adolescents with cancer: challenges for the twenty-first century. J Clin Oncol. 2010;28:2625–34.
5. Balwierz W, Wieczorek A, Klekawka T, Garus K, Bolek-Marzec K, Perek D, et al. Treatment results of children with neuroblastoma: report of Polish Pediatric Solid Tumor Group. Przegl Lek. 2010;67:387–92.
6. Perwein T, Lackner H, Sovinz P, Benesch M, Schmidt S, Schwinger W, et al. Survival and late effects in children with stage 4 neuroblastoma. Pediatr Blood Cancer. 2011; doi:10.1002/pbc.23036.
7. Boubaker A, Bischof Delaloye A. Nuclear medicine procedures and neuroblastoma in childhood. Their value in the diagnosis, staging and assessment of response to therapy. Q J Nucl Med. 2003;47:31–40.
8. Schmidt M, Simon T, Hero B, Schicha H, Berthold F. The prognostic impact of functional imaging with (123)I-mIBG in patients with stage 4 neuroblastoma >1 year of age on a high-risk treatment protocol: results of the German Neuroblastoma Trial NB97. Eur J Cancer. 2008;44:1552–8.
9. Boubaker A, Bischof Delaloye A. MIBG scintigraphy for the diagnosis and follow-up of children with neuroblastoma. Q J Nucl Med Mol Imaging. 2008;52:388–402.
10. Gordon I, Peters AM, Gutman A, Morony S, Dicks-Mireaux C, Pritchard J. Skeletal assessment in neuroblastoma – the pitfalls of iodine-123-MIBG scans. J Nucl Med. 1990;31:129–34.
11. Biasotti S, Garaventa A, Villavecchia GP, Cabria M, Nantron M, De Bernardi B. False-negative metaiodobenzylguanidine scintigraphy at diagnosis of neuroblastoma. Med Pediatr Oncol. 2000;35:153–5.
12. Kushner BH, Yeh SD, Kramer K, Larson SM, Cheung NK. Impact of metaiodobenzylguanidine scintigraphy on assessing response of high-risk neuroblastoma to dose-intensive induction chemotherapy. J Clin Oncol. 2003;21:1082–6.
13. Shulkin BL, Hutchinson RJ, Castle VP, Yanik GA, Shapiro B, Sisson JC. Neuroblastoma: positron emission tomography with 2-[fluorine-18]-fluoro-2-deoxy-D-glucose compared with metaiodobenzylguanidine scintigraphy. Radiology. 1996;199:743–50.
14. Kushner BH. Neuroblastoma: a disease requiring a multitude of imaging studies. J Nucl Med. 2004;45:1172–88.
15. Sharp SE, Shulkin BL, Gelfand MJ, Salisbury S, Furman WL. 123I-MIBG scintigraphy and 18F-FDG PET in neuroblastoma. J Nucl Med. 2009;50:1237–43.
16. Brodeur GM, Pritchard J, Berthold F, Carlsen NL, Castel V, Castelberry RP, et al. Revisions of the international criteria for neuroblastoma diagnosis, staging, and response to treatment. J Clin Oncol. 1993;11:1466–77.
17. Matthay KK, Shulkin B, Ladenstein R, Michon J, Giammarile F, Lewington V, et al. Criteria for evaluation of disease extent by (123)I-metaiodobenzylguanidine scans in neuroblastoma: a report for the International Neuroblastoma Risk Group (INRG) Task Force. Br J Cancer. 2010;102:1319–26.
18. Olivier P, Colarinha P, Fettich J, Fischer S, Frokier J, Giammarile F, et al. Guidelines for radioiodinated MIBG scintigraphy in children. Eur J Nucl Med Mol Imaging. 2003;30:B45–50.
19. Stauss J, Franzius C, Pfluger T, Juergens KU, Biassoni L, Begent J, et al. Guidelines for 18F-FDG PET and PET-CT imaging in paediatric oncology. Eur J Nucl Med Mol Imaging. 2008;35:1581–8.
20. Vik TA, Pfluger T, Kadota R, Castel V, Tulchinsky M, Farto JC, et al. (123)I-mIBG scintigraphy in patients with known or suspected neuroblastoma: Results from a prospective multicenter trial. Pediatr Blood Cancer. 2009;52:784–90.
21. Jacobson AF, Deng H, Lombard J, Lessig HJ, Black RR. 123I-meta-iodobenzylguanidine scintigraphy for the detection of neuroblastoma and pheochromocytoma: results of a meta-analysis. J Clin Endocrinol Metab. 2010;95:2596–606.
22. Pfluger T, Schmied C, Porn U, Leinsinger G, Vollmar C, Dresel S, et al. Integrated imaging using MRI and 123I metaiodobenzylguanidine scintigraphy to improve sensitivity and specificity in the diagnosis of pediatric neuroblastoma. AJR Am J Roentgenol. 2003;181:1115–24.
23. Connolly LP, Drubach LA, Ted Treves S. Applications of nuclear medicine in pediatric oncology. Clin Nucl Med. 2002;27:117–25.
24. Kushner BH, Yeung HW, Larson SM, Kramer K, Cheung NK. Extending positron emission tomography scan utility to high-risk neuroblastoma: fluorine-18 fluorodeoxyglucose positron emission tomography as sole imaging modality in follow-up of patients. J Clin Oncol. 2001;19:3397–405.
25. Shulkin BL, Shapiro B. Current concepts on the diagnostic use of MIBG in children. J Nucl Med. 1998;39:679–88.
26. Pfluger T, Schmid I, Coppenrath E, Weiss M. Modern nuclear medicine evaluation of neuroblastoma. Q J Nucl Med Mol Imaging. 2010;54:389–400.
27. McDowell H, Losty P, Barnes N, Kokai G. Utility of FDG-PET/CT in the follow-up of neuroblastoma which became MIBG-negative. Pediatr Blood Cancer. 2009;52:552.

28. Kushner BH, Kramer K, Modak S, Cheung NK. Sensitivity of surveillance studies for detecting asymptomatic and unsuspected relapse of high-risk neuroblastoma. J Clin Oncol. 2009;27:1041–6.
29. Colavolpe C, Guedj E, Cammilleri S, Taieb D, Mundler O, Coze C. Utility of FDG-PET/CT in the follow-up of neuroblastoma which became MIBG-negative. Pediatr Blood Cancer. 2008;51:828–31.
30. Frappaz D, Bonneu A, Chauvot P, Edeline V, Giammarile F, Siles S, et al. Metaiodobenzylguanidine assessment of metastatic neuroblastoma: observer dependency and chemosensitivity evaluation. The SFOP Group. Med Pediatr Oncol. 2000;34:237–41.
31. Taggart DR, Han MM, Quach A, Groshen S, Ye W, Villablanca JG, et al. Comparison of iodine-123 metaiodobenzylguanidine (MIBG) scan and [18F]fluorodeoxyglucose positron emission tomography to evaluate response after iodine-131 MIBG therapy for relapsed neuroblastoma. J Clin Oncol. 2009;27:5343–9.
32. Goo HW. Whole-body MRI of neuroblastoma. Eur J Radiol. 2010;75:306–14.